Separating the effects of climate change and human activities on drought propagation via a natural and human-impacted catchment comparison method

Menghao Wang[a, b], Shanhu Jiang[a, b*], Liliang Ren[a, b*], Chong-Yu Xu[c], Lucas Menzel[d], Fei Yuan [a, b], Qin Xu[e], Yi Liu[b], Xiaoli Yang[b]

[a]*State Key Laboratory of Hydrology-Water Resources and Hydraulic Engineering, Hohai University, Nanjing 210098, China*

[b]*College of Hydrology and Water Resources, Hohai University, Nanjing 210098, China*

[c]*Department of Geosciences, University of Oslo, Oslo, Norway*

[d]*Department of Geography, Professorship in Hydrology and Climatology, Heidelberg University, Heidelberg D-69120, Germany*

[e]*Nanjing Hydraulic Research Institute, Nanjing 210000, China*

Submitted to *Journal of Hydrology*

*Corresponding author:

Professor Shanhu Jiang and Liliang Ren

State Key Laboratory of Hydrology-Water Resources and Hydraulic Engineering, Hohai University, Nanjing 210098, China

Email: hik0216@hhu.edu.cn; njrll9999@126.com

Abstract

It is crucial to investigate how a precipitation deficit is transformed into hydrological drought and how climate change and human activities affect this transformation process, which is helpful to gain a deep understanding of drought propagation process in this changing environment. This study proposed an observation-based natural and human-impacted catchment comparison method to assess the impacts of climate change and human activities on propagation from meteorological drought to hydrological drought. The method mainly consists of the following three steps: (1) selection of natural catchments through analysis of trends and change points of hydro-meteorological data, as well as statistics analysis of human influence based on land use and socio-economic indicators data sets; (2) calculation of drought propagation characteristics (e.g., drought severity, duration, and propagation time) based on run theory and the Pearson correlation coefficient; and (3) comparison of drought propagation characteristics of natural catchments between undisturbed and disturbed periods to identify the impacts of climate change on drought propagation, and comparison of the propagation characteristics between natural and human-impacted catchments during the disturbed period to investigate human influence on drought propagation. The Laohahe basin (with eleven sub-catchments), located in northern China, was evaluated via the proposed procedure, and standardized precipitation index (SPI) and standardized runoff index (SRI) were used to characterize meteorological and hydrological droughts, respectively. The results demonstrate that the proposed method is suitable tool for distinguishing natural and human-impacted catchments, and separating the impacts of climate change and human activities on drought propagation. Furthermore, the comparison results of different schemes show that climate change accelerates the propagation from meteorological drought to hydrological drought in the Laohahe basin, shortening it by approximately 3 months. Human activities, however, disturb and then delay the natural propagation from meteorological drought to hydrological drought, retarding it by 11–12 months. Although the Laohahe basin was selected as a case study in this paper, the proposed method can be applied in other regions as well to improve drought prediction and water resources management.

Keywords: Meteorological drought; Hydrological drought; Drought propagation; Climate change; Human activities; Nonparametric Standardized Drought Index

1. Introduction

Drought is widely recognized as a complex, multidimensional phenomenon that occurs in most parts of the world (Wang et al., 2020; Tijdeman and Menzel, 2020; Jiang et al., 2019; Van Loon et al., 2016; Barker et al., 2016; Sheffield et al., 2012; Dai, 2011; Mishra and Singh, 2010). Drought starts with negative hydro-climatic signals (i.e., meteorological drought) and propagates through interconnected hydrological subsystems such as soil systems (i.e., soil moisture drought), surface water systems and groundwater bodies (i.e., hydrological drought), and then extends from water stored in the landscape to vegetation stress (i.e. agriculture and natural plants) and human water demand (i.e., socio-economic drought) (Apurv and Cai, 2020). This concept is referred to as drought propagation (Eltahir and Yeh, 1999; Peters et al., 2003), which is commonly characterized by four features: pooling, attenuation, lag, and lengthening (Van Loon, 2015). Many investigations have examined the driving mechanisms and controlling factors of drought propagation, such as climate, catchment properties, and human influences (Peters et al., 2003; Tallaksen et al., 2009; Vidal et al., 2010; Van Loon and Van Lanen., 2012; Tijdeman et al., 2018).

Under global change, the driving force for the occurrence, development, spread, and evolution of drought has gradually transitioned from a single natural factor (i.e., climate variability) to a combination of "natural-human" factors (i.e., climate change and human activities) (Van Loon et al., 2016; Jiang et al., 2019). Severe recent drought events that occurred in California, China, Spain and Australia cannot be viewed as purely natural hazards (Lorenzo-Lacruz et al., 2013; AghaKouchak et al., 2015). Anthropogenic changes to the land surface have significantly altered hydrological processes, mainly including surface runoff and water storage, which in turn affect the development of drought (Van Loon et al., 2016; Huang et al., 2017). Therefore, it is important to investigate how climate change and human activities alter drought propagation from meteorological to hydrological drought, which is helpful for improving drought prediction and water resources management.

For evaluating diverse drought events, a number of drought indices have been developed and then applied widely across the world in recent decades (Wells et al, 2004; Shukla and Wood, 2008; López-Moreno et al., 2013; Farahmand and AghaKouchak, 2015). Among all the drought indices, the standard precipitation index (SPI) and the standard runoff index (SRI) have been used the most widely for evaluation of meteorological and hydrological drought, respectively, because they have the following advantages: robust and flexible time scale, relatively simple calculation, and limited data requirement. However, SPI and SRI usually rely on different parametric distribution functions to fit the corresponding sample data (i.e., precipitation and runoff), which will result in different fitting behaviours and then impact the statistical consistency and comparability of these two drought indices (Farahmand and AghaKouchak, 2015). Furthermore, because the complicated interactions among surface water, atmosphere, vegetation, soil, and groundwater have substantial impacts on hydrologic processes, different catchments may have different representative parametric distribution functions, which will impact the comparability of drought indices between different catchments. Hence, a generalized framework for deriving non-parametric standardized drought indicators (Farahmand and AghaKouchak, 2015; Huang et al., 2015) was used in this study to calculate the non-parametric SPI and SRI series, because it leads to statistically consistent drought indicators based on different climate and land-surface variables without assuming representative parametric distributions, which can ensure the comparability of different drought indexes in different catchments. Moreover, the run theory (Yevjevich, 1967), a widely used method for extracting drought characteristics, was applied in this study. If the drought index in a certain period remain below the threshold (e.g., drought index = 0) of the run theory, the run during this period will be regarded as a drought event, and the corresponding drought duration and severity can be identified.

Currently, commonly used methods for studying drought propagation can be categorized into two groups, i.e., those using statistical analysis (Lorenzo-Lacruz et al., 2013; López-Moreno et al., 2013; Veettil et al., 2018; Konapala and Mishra, 2020; Veettil and Mishra, 2020; Apurv and Cai, 2020) and those using hydrologic models (Longobardi and Van Loon, 2018; Tallaksen et al., 2009; Van Lanen et al., 2013; Van Loon and Van Lanen, 2012). Methods based on hydrological models are often used to explore the physical mechanisms of drought propagation. Statistical analysis methods, such as correlation analysis and machine learning are usually applied to identify the climate and watershed properties that control drought propagation. In this study, the widely used statistical method, i.e., Pearson correlation coefficient (PCC) proposed by Pearson (1895), was selected to quantitatively identify the correlation between the SRI and the SPI series, and the SPI accumulation period with the strongest PCC was used as an indicator of the drought propagation time (Barker et al., 2016; Wu et al., 2018).

In addition, a common method for assessing the impacts of climate change and human activities on hydrological processes is to find a natural reference catchment and compare the hydrological processes in natural catchments with those in impacted (or managed) catchments to distinguish the effects of different factors (Ficklin et al., 2018; Roodari et al., 2021). There are several approaches that focus on finding natural catchments from observation data and perform comparison analysis, such as the following six: (1) the “large-scale screening” approach (Wagener et al., 2010), (2) the “paired catchments” approach (Van Loon et al., 2019), (3) the “observation-modelling” approach (Van Loon and Van Lanen, 2013), (4) the “upstream-downstream” approach (Rangecroft et al., 2019), (5) the “pre-post-disturbance” approach (Liu et al., 2016) and (6) the “tributary-comparison” approach (Li et al., 2020; Wang et al., 2020). Downsides of the first two methods are that they require a large number of catchments with long time series of hydrological data (Li et al., 2020; Van Loon et al., 2019). Downsides of the third method are that the simulated data often have uncertainties and a pre-disturbed period is needed for calibration to reduce those (Rangecroft et al., 2019; Roodari et al., 2021). Meanwhile, another disadvantage of the third method is that before a model can be used in climate change studies, we must first ensure that it is climate transferable (Stephens et al., 2021). The approaches (4) and (5) either have uncertainties that come from the possible non-linear relationship between the upstream and downstream gauging stations (Van Loon et al., 2019) or have some difficulties separating the human influence from climatic variability (Peñas et al., 2016). The “tributary-comparison” approach (Li et al., 2020) establishes an indicator system for the selection of natural reference tributary according to the drought propagation intensity, reservoir, and land use conditions, but does not consider socio-economic indicators.

In general, most of existing studies did not establish a unified index system to divide natural and human-impacted catchments. A few methods established index systems but do not consider the socio-economic indicators closely related to human activities (e.g., GDP and population density). According to the above limitations, the present study establishes a preliminary indicator system to evaluate the land use data and socio-economic indicators (i.e., GDP, population, and night light density) to quantify human influence, and combines its results with the analysis results of trends and change points of hydro-meteorological data to select natural catchments. This is a novelty of the study. Then, this study proposed a natural and human-impacted catchment comparison method to use observation data to separate the effects of climate change and human activities on drought propagation, so as to ensure the climate transferability of this method. The whole calculation framework mainly consists of three steps: (1) selecting natural catchments through combing the analysis results of hydrological variations with the quantification results of human influence; (2)

calculating drought propagation characteristics (e.g., drought severity , duration, and propagation time) based on the Pearson correlation coefficient and run theory method; and (3) comparison of drought propagation characteristics of natural catchments between undisturbed and disturbed periods to identify the impacts of climate change on drought propagation, and comparison of the ones between natural and human-impacted catchments during the disturbed period to investigate human influence on drought propagation. The Laohahe basin located in northern China with a high degree of human influence, was chosen as the study area to perform the proposed method.

2. Study area and data source

2.1 Study area

The Laohahe basin, located in a typical semiarid region of northeast China (41.0°N–42.75°N, 117.25°E–120°E), covers an area of 18,112 km^2, with the Xinglongpo hydrological station at the basin outlet (as shown in Fig. 1). The elevation of the Laohahe basin ranges between 2054 m and 427 m above mean sea level, with a generally declining trend from southwest to northeast. Summer is the main rainy season and approximately 60%–70% of the annual precipitation occurs during June–August. Runoff in the Laohahe basin exhibits the similar seasonality, with about 70% of the annual runoff concentrated in June–September (Yong et al., 2013; Wang et al. 2020). Similar to other semiarid basins, the annual potential evapotranspiration (PET) of the

Laohahe basin exceeds annual precipitation, and about 60%–70% of the annual PET focus on April–August. Sunshine duration, an insolation variable closely related to PET, shows a similar seasonality with PET, i.e., the sunshine hours in March–August are significant higher than those in other months.

In this study, we selected 11 catchments (Fig. 1), including seven headwater catchments from north to south (catchments 1–7, independent of each other), three midstream catchments (catchments 8–10, indicated with the red solid line boundaries in Fig. 1) and the whole basin (i.e., catchment 11, including all the sub-catchments). Table 1 lists the geographic and hydrological information of these 11 catchments. The ranges of average annual precipitation and runoff in these catchments are 390–580 mm and 20–120 mm, respectively, with a gradual declining trend from south (catchments 4–7) to north (catchments 1–3 and 8–11). It is worth noting that Jiang et al. (2011) found that human activities were the main factors (with contributions of 89–93%) contributing to the runoff decrease in the Laohahe basin after 1979 and recent studies shows the decreasing trend of runoff in this basin is continuing (Yong et al., 2013; Liu et al., 2016; Jiang et al., 2019; Wang et al., 2020).

Insert Figure 1 about here

Insert Table 1 about here

2.2 Data source

The data used in this study mainly consists of three parts: hydro-meteorological data, agricultural and industrial production data, and remote sensing inversion and reanalysis data.

(1) Monthly precipitation data measured by 52 rain gauges, monthly streamflow data measured by 11 hydrological stations, and monthly meteorological data measured by 7 meteorological stations (including maximum, mean, and minimum air temperatures, wind speed, and insolation) from 1964 to 2016 were provided by the Water Resources Department of the Inner Mongolia Autonomous Region. Precipitation data were interpolated through the inverse distance weighting (IDW) method to calculate the areal average of precipitation in each catchment. Meteorological data were interpolated through the (IDW) method to calculate the areal average of PET though the Penman-Monteith equation (Allen et al., 1998), whilst corresponding actual evaporation was calculated through water balance equation (Yong et al., 2013; Huang et al., 2017). Moreover, monthly streamflow were divided by the catchment area to get the runoff (areal average depth) in each catchment (Shukla and Wood, 2008; Wu et al., 2018) to compare with the precipitation and PET. Annual human water use data of each catchment during 2006–2016 and information of three large reservoirs were also provided by the Water Resources Department of the Inner Mongolia Autonomous Region.

(2) Agricultural and industrial production data for the Laohahe basin during 1964-2016, including the annual food production, number of livestock, irrigated area, and Gross Industrial Product (GIP) were collected from the local statistical bureau website (http://tjj.chifeng.gov.cn/). These data are selected to reflect the temporal changes of the degree of human agricultural and industrial activities in the Laohahe basin during the entire study period (1964-2016).

(3) Remote sensing inversion and reanalysis data used in this study and their detail information are listed in Table 2. Large-scale climate indices, i.e., annual ENSO, PDO, AO, and sunspot data were applied in this study to investigate the impact of climate change on drought propagation. Surface soil moisture and GRACE data were used to analyse the surface soil moisture and terrestrial water storage anomalies (TWSA) of the study area. Grid remote sensing inversion and reanalysis data sets including land use, population density, GDP density, and night light density were collected to analyse the human influence on the study area and then to support for the selection of natural catchments.

Insert Table 2 about here

3. Methodology

In this study, we proposed an observation-based natural and human-impacted catchment comparison method (illustrated in Fig. 2) for assessing the impacts of climate change and human activities on drought propagation from meteorological to hydrological drought. The three steps of the proposed method are described below.

Insert Figure 2 about here

(1) Selection of natural catchments

The first step focuses on the selection of natural catchments. A preliminary knowledge of the hydrological regime changes in each catchment can be identified based on the results of MMK trend analyses and change point tests of annual precipitation, PET, and runoff during the entire research period. In addition, the precipitation-runoff double cumulative curve (DCC) reflects the consistency of precipitation and runoff series and is helpful to identify change points visually. Note that, based on previous studies (Wang et al., 2020; Jiang et al., 2019; Van Loon and Van Lanen, 2013), the entire research period is usually divided into two parts by the first change point for further comparison schemes design: undisturbed period (the period before the change point) and disturbed period (the period after the change point).

Furthermore, socio-economic indicators (including average population, GDP, and night light density) and land use data for each catchment are collected and then are used to calculate human influence scores through an indicator system. Finally, according to the analysis results of trend and change point of hydro-meteorological variables, human influence scores, and reservoir information, all the studied catchments can be divided into two types: natural catchments and human-impacted catchments.

(2) Calculation of drought propagation characteristics

The second step is the calculation of drought propagation characteristics, including drought duration, severity, and propagation time. Run theory is first used to identify drought duration and severity of SPI and SRI at different timescales (e.g., SPI-*x* and SRI-*x*, *x*=1, 3, 12 months). In addition, a comparison between SRI and SPI provides an indication of the time taken for precipitation deficits to propagate through the hydrological cycle to hydrological drought (Barker et al., 2016). In this study, SPI accumulation periods of 1–48 months (SPI-*n*, *n*=1, 2, ..., 48 months) and SRI-1 time series were cross-correlated using the PCC to investigate the most appropriate propagation time from meteorological to hydrological drought. The SPI accumulation period with the strongest correlation with SRI-1 was regarded as the appropriate drought propagation time. Where SRI-1 was most strongly correlated with short SPI accumulation periods, the propagation time was also short, and vice versa.

(3) Assessment of the impacts of different factors on drought propagation

In the final step, different comparison schemes (as shown in step 3 in Fig. 2) are designed to assess the impacts of climate change and human activities on drought propagation. In comparison Ⅰ, propagation time of natural and human-impacted catchments during the undisturbed period are compared to investigate the similarity of drought propagation pattern in these two types of catchments. In comparison II, for a natural catchment, the difference of drought propagation time between undisturbed and disturbed periods can reflect the impact of climate change on drought propagation under the condition that the underlying surface properties (e.g., catchment area, soil types, vegetation types, etc.) remain approximately unchanged. In comparison Ⅲ, natural and human-impacted catchments are all affected by climate change in the disturbed period, and differences in propagation characteristics between natural and human-impacted catchments should be attributed to effects of human activities. The concept underlying this approach and the methods used are described in detail in the following sections.

3.1 Trend and change point analysis

3.1.1 Modified Mann-Kendall (MMK) trend test method

The traditional Mann-Kendall (MK) trend test method, recommended by the World Meteorological Organization, is a widely used nonparametric method for trend tests of time series. However, Hamed and Rao (1998) found that the persistence of hydro-meteorological series impacts the robustness of the MK test results. Then, they used lag-*i* autocorrelation to remove the persistence to make the test result more reliable and robust, which is known as the modified Mann-Kendall (MMK) trend test method. In this study, therefore, we adopted the MMK method to identify the trend of the SPI and SRI series. The detailed computational processes can be found in Hamed and Rao (1998) and Huang et al. (2015).

3.1.2 Change point test methods

The Pettitt test (Pettitt, 1979) is a widely used nonparametric test method to determine a change point of hydro-meteorological variable time series at a given significance level (e.g., α = 0.05). This approach is based on rank statistics and considers a time series as two samples represented by x_1, x_2, ..., x_t and x_{t+1}, ..., x_N (N is the length of the time series). The Pettitt indices $U_{t,N}$ can be calculated as follows:

$$U_{t,N} = \sum_{j=1}^{t}\sum_{i=1}^{N}\operatorname{sgn}\left(x_j - x_i\right),\ (t = 1, 2, ..., N) \tag{1}$$

where,

$$\operatorname{sgn}(\theta) = \begin{cases} +1, & \theta > 0 \\ 0, & \theta = 0 \\ -1, & \theta < 0 \end{cases} \tag{2}$$

Then, we can calculate the series of probabilities of change points for each time step:

$$p \cong 1 - \exp\left[\frac{-6\left(U_{t,N}\right)^2}{N^3 + N^2}\right] \tag{3}$$

In addition to the Pettitt test, the heuristic segmentation method and the precipitation- runoff double cumulative curve (DCC) method were applied in this study to ensure robustness of the change point test results. The heuristic segmentation method, proposed by Bernaola-Galvan et al. (2001), is developed on the basis of the sliding T test and has been widely used to identify change points of nonlinear and non-stationary time series. Because the detailed calculation processes of the method are well introduced in Bernaola-Galvan et al. (2001) and Huang et al. (2015), they are omitted in this study for the sake of brevity.

The precipitation and runoff double cumulative curve (DCC) method can visually illustrate the consistency of precipitation and runoff data (Jiang et al., 2019; Wang et al., 2020). Generally, a change in the gradient of the curve may infer that the characteristics of precipitation or runoff have changed, and the inflection point of the curve is generally regarded as a change point.

3.2 Establishment of an indicator system for accessing human influence

In the proposed method (as shown in Step 1 in Fig. 2), we selected four representative socio-economic indicator data sets to analyse human influence, including GDP, population, night light density data sets and land use data set (listed in Table 2). Firstly, GDP and population density data sets can intuitively reflect the economic activities and human settlement conditions, respectively, so they are often used to evaluate the intensity of regional human impacts (Woolmer et al., 2008; Yue et al., 2014). Secondly, remotely sensed night time lights dataset is widely used to characterize trends in urban sprawl over time, and can monitor dynamics in human settlement and economic activity at regional to global scales (Ma et al., 2012). Finally, the proportion of cropland and urban land is closely related to agriculture, residential, and industrial development, and is also usually used to reflect the degree of human influence in the basin (Li et al., 2020; Wang et al., 2020).

Based on the above four data sets, an indicator system is built to quantify human influence and then to support for the division of natural and human-impacted catchments. In this indicator system, we used a method similar to that of Sanderson et al. (2002) and Woolmer et al. (2008) to combine the four datasets. We express each dataset as overlaying grids at a resolution of about 1 square kilometre (km^2) and scored each dataset to reflect their contribution to human influence. Sum of the scores of all indicators are the human influence index (HI). These scoring criteria are based on published scientific studies (as summarized in Table 3). Higher scores indicate greater human influence and vice versa. The areal average HI scores of each catchment can be calculated as follows.

$$HI_k = \sum_{i=1}^{N} HI_i \Big/ N \tag{4}$$

where HI_k means the areal average HI score of a catchment ($k = 1, 2, \ldots, 11$), HI_i means the HI score of a grid cell in the catchment, N is the total number of grids in the catchment.

Insert Table 3 about here

3.3 Drought calculation

3.3.1 Nonparametric standardized drought index

For standardized drought index, parametric distribution functions are commonly adopted to fit the probability distribution of hydro-meteorological variables, including precipitation, soil moisture, and runoff. Then, the cumulative probability is converted to the cumulative distribution function (CDF) of the standard normal distribution. Finally, the standardized index (SI) value is calculated through the inverse of the standard normal distribution (Farahmand and AghaKouchak, 2015; Huang et al., 2015). For the nonparametric standardized drought index, the empirical probability that is distribution-free can replace the cumulative probability to derive a nonparametric SI without having to assume representative parametric distributions. Here, we take a runoff series ($X=\left[x_1,x_2,\ldots,x_n\right]$) as an example to derive its probability distribution.

$$p(x_i)=\frac{i-0.44}{n+0.12} \tag{5}$$

where i is the rank of the runoff value x_i from the smallest, n is the sample size of the runoff series, and $p(x_i)$ is the corresponding empirical probability. The outputs of Eq. (5) can be transformed to a SI as follows:

$$SI=\phi^{-1}(p) \tag{6}$$

where, ϕ is the standard normal distribution function, and p is the probability derived from Eq. (5). More detailed calculation processes of nonparametric standardized drought indicators can be found in Farahmand and AghaKouchak (2015).

One advantage of the SI is its ability to investigate drought at different timescales. In this study, different timescales of nonparametric standardized precipitation index

(SPI-*x*) and standardized runoff index (SRI-*x*) were calculated to describe short- or long-term meteorological and hydrological drought. For example, SPI-3 and SRI-12 denote a 3-month precipitation accumulation period and a 12-month runoff accumulation period, respectively (Wu et al., 2018). The drought grade is divided into five levels based on previous studies (Vicente-Serrano et al, 2012): SPI (or SRI) > 0, –1 ≤ SPI < 0, –1.5 ≤ SPI < –1.0, –2.0 ≤ SPI < –1.5, and SPI ≤ –2, which correspond to no drought, mild drought, moderate drought, severe drought, and extreme drought, respectively.

3.3.2 Run theory

In run theory (proposed by Yevjevich, 1967), drought events are defined as a period where indicator values are continuously below a certain threshold (Huang et al., 2015; Wu et al., 2018), so a threshold level (TL) of 0 is selected in this study to determine drought conditions. The calculation process of these characteristics is as follows (using SPI as an example):

The drought state (*DS*) is given by:

$$
\begin{aligned}
Ds(t) &= 1, \text{ for } SPI(t) < TL \\
&= 0, \text{ for } SPI(t) \geq TL
\end{aligned} \tag{7}
$$

The drought severity (*S*) per time step is defined by:

$$
\begin{aligned}
S(t) &= TL - SPI, \text{ for } Ds(t) = 1 \\
&= 0, \qquad\qquad \text{for } Ds(t) = 0
\end{aligned} \tag{8}
$$

The drought duration (D) and severity (S) for drought event i are calculated with:

$$D_i = \sum_{t=F_i}^{L_i} Ds(t) \tag{9}$$

$$S_i = \sum_{t=F_i}^{L_i} S(t) \tag{10}$$

where $SPI(t)$ is the SPI value at a given time t; TL is the threshold level (in this study, we set the TL to 0); $Ds(t)$ is a binary variable indicating if drought occurs at a given time t; D_i is the drought duration of event i; S_i is the total drought severity of event i; and F_i and L_i are the first- and last- time steps of event i.

3.4 Correlation analysis

3.3.1 Pearson correlation coefficient

The Pearson correlation coefficient (PCC), developed by Pearson (1895), has been widely used throughout hydrological correlation analyses. In this study, we used the PCC to identify the correlation between the SRI and the SPI at different timescales. According to previous studies (Barker et al., 2016; Wu et al., 2018), the SPI accumulation period with the strongest PCC is used as an indicator for drought propagation. The PCC is calculated as follows:

$$PCC = \frac{\sum_{i=1}^{n}(\varphi_i - \overline{\varphi})(\omega_i - \overline{\omega})}{\sqrt{\sum_{i=1}^{n}(\varphi_i - \overline{\varphi})^2}\sqrt{\sum_{i=1}^{n}(\omega_i - \overline{\omega})^2}},\ i = 1, 2, \ldots, n \tag{11}$$

where φ_i and ω_i denote two time series, and $\overline{\varphi}$ and $\overline{\omega}$ denote the average values of the two series. The PCC ranges from +1 to –1, where +1, 0, and –1 indicate total positive linear correlation, no linear correlation, and total negative linear correlation, respectively.

3.4.2 Cross-wavelet analysis

Cross-wavelet analysis (Hudgins and Huang, 1996; Torrence and Compo, 1998) is a technique coupled with cross-spectrum analysis and wavelet transform. This method can effectively identify the correlation between two time series in the time-frequency domain. The cross-wavelet transforms (CWT) of two specific time series (e.g., x_n and y_n) can be defined as $W^{XY} = W^X W^{Y*}$, where * denotes their complex conjugation. The cross-wavelet power can be expressed as $|W^{XY}|$, and the complex argument arg (W^{xy}) can be regarded as the local relative phase between x_n and y_n in the time-frequency domain. The theoretical distribution of the cross-wavelet power of the two time series is defined as follows:

$$D\left(\frac{\left|W_n^X(s)W_n^Y*(s)\right|}{\sigma_X\sigma_Y} < p\right) = \frac{Z_v(p)}{v}\sqrt{P_k^X P_k^Y} \tag{12}$$

where $Z_v(p)$ is the confidence level associated with probability p for a probability distribution function defined by the square root of the product of two χ^2 distributions. P_k^X and P_k^Y are background power spectra of time series x_n and y_n, respectively (Grinsted et al., 2004).

4. Results

4.1 Selection of natural catchments

Fig. 3 visually shows the significant changes in the relationship between precipitation and runoff in the 11 selected catchments. Except for the YSWZ, JS, and XQ catchments (Fig. 3(c), (d), and (f)), the gradients of the runoff accumulation curve were significantly different from those of the precipitation accumulation curve for the remaining eight catchments (Fig. 3(a), (b), (e), and (g)–(k)) after 1979 and/or 1999. Furthermore, Table 4 shows the results of the MMK trend analysis and change point tests of annual precipitation, PET, and runoff for the 11 selected catchments during the period from 1964 to 2016. Expect for PET in the TPZ catchment, which showed an upward trend, PET and precipitation of all the catchments showed a downward trend without reaching a significant level (α = 0.05). There were also no significant (α = 0.05) change points in the precipitation and PET series for the 11 catchments. Different from the above two variables, runoff in most catchments showed a significant downward trend (α = 0.05), except for the YSWZ, JS, and XQ catchments. For the eight catchments with significant downward trends in runoff series, change points were identified in 1979 through Pettitt and heuristic segmentation test methods. Based on the results of trend and change point analyses, we found that the relationship between precipitation and runoff for the YSWZ, JS, and XQ catchments was relatively stable and consistent throughout the entire research period (1964–2016).

Insert Figure 3 about here

Insert Table 4 about here

Fig. 4 shows the temporal changes of socio-economic indicators (average population, GDP, and night light density), proportion of cropland and urban land, and human influence scores for the catchments in the Laohahe basin. For the average population density (Fig. 4(a)), CF, TPZ, and XLP catchments show a slight downward trend during 2000-2015, while the other catchments remain almost unchanged. For the average GDP density (Fig. 4(b)), all catchments show an upward trend, but the growth rate of the XLP and CF catchments is significantly faster than that of the remain catchments during 2000-2015. Similarly, night light density also has an increasing trend for all catchments, but CF, TPZ, and XLP catchments are obviously growing faster than the other catchments. For the land use situation, i.e., proportion of cropland and urban land during 1980-2015, which are directly related to human activities, shows a slight upward trend in XCZ, XD, CF, TPZ, and XLP catchments, but remain constant in the other catchments. Finally, the human influence scores, which are calculated based on the above four indictors, increased rapidly in CF, TPZ, and XLP catchment, but increased slowly in remain catchments. Table 5 indicates that areal average human influence scores of the YSWZ, JS, and XQ catchments during 2000-2015 were the three lowest, while those of the other catchments all exceeded these three catchments.

Insert Figure 4 about here

Furthermore, Fig. 5 shows the spatial distributions of socio-economic indicators, land use data, and human influence scores. Generally, all these indicators showed an upward trend from headwater catchments (catchments 1–7, i.e., CTL, XJD, YSWZ, JS, XCZ, XQ, and DZ catchments) to midstream catchments (catchments 8–10, i.e., XD, CF, and TPZ catchments) and downstream catchments (catchment 11, i.e., XLP catchment). In summary, combined with results of trend and change points analysis of hydrological variables, human influence scores, and reservoir information (listed in Table 5), YSWZ, JS, and XQ catchments can be selected as natural catchments, because the three catchments have consistent relationships between precipitation and runoff, and are affected by weak human activities (i.e., low human influence scores and no reservoir regulations). Remain eight catchments are either affected by reservoir regulations or strong human activities (i.e., high human influence scores), so they are classified into human-impacted catchments. Meanwhile, according to the analysis results of the first change point for each catchment, and temporal change of socio-economic indicators and land use data, the entire research period can be divided into two periods: the undisturbed period (1964–1979) and the disturbed period (1980–2016) for further design of comparison scheme.

Insert Figure 5 about here

Insert Table 5 about here

4.2 Propagation from meteorological to hydrological drought

To identify propagation from meteorological to hydrological drought in the Laohahe basin, we first used the MMK method to analyse the trends of these two categories of drought during 1964−2016 for 11 catchments in the Laohahe basin (Fig. 6) based on the SPI and SRI measured over 1-, 3-, and 12-month timescales. These three timescales represent monthly, seasonal, and annual drought and can adequately depict the evolution of drought in the study area. Then, drought evolutionary characteristics for the undisturbed and disturbed periods were calculated through run theory, including drought duration and severity (Fig. 7 and Table 6). In addition, the propagation time from meteorological to hydrological drought was identified by the SPI accumulation period (SPI-n) most strongly correlated with SRI-1 based on the PCC (Fig. 8 and Fig. 9).

4.2.1 Trend analysis of meteorological and hydrological drought

Fig. 6 shows the trends of long-term SPI and SRI time series at 1-, 3-, and 12-month scales in 11 catchments in the Laohahe basin during the period 1964–2016. All catchments except DZ catchment showed downward trends in SPI-1 and SPI-3, but none of these downward trends were significant (Fig. 6(a) and (b)). SPI-12 in most catchments, except for the JS and XCZ catchments, exhibited significant ($\alpha = 0.05$) downward trends (Fig. 6(c)), with the largest Z values for SPI-12 in the XD catchment (–4.18). For hydrological drought, all catchments except YSWZ, JS, and XQ showed significant downward trends ($\alpha = 0.05$) in the SRI-1, SRI-3, and SRI-12 time series (Fig. 6(d)-(e)). XD catchment experienced the worst hydrological drought, with Z values of –8.79, –11.16, and –6.04 for SRI-1, SRI-3, and SRI-12, respectively. In general, the SRI series measured over 1-, 3-, and 12-month time scales showed a clear spatial distribution, with stronger downward trends in the midstream and downstream catchments (i.e., XD, CF, TPZ, and XLP catchments) than in the headwater catchments (i.e., CTL, XJD, YSWZ, JS, XCZ, XQ, and DZ catchments).

Insert Figure 6 about here

4.2.2 Evolutionary characteristics of meteorological and hydrological drought

As shown in Fig. 7, drought severity calculated from SPI-3 and SRI-3 series are selected as an example to show drought propagation characteristics during different periods. In the undisturbed period, for each catchment except XQ, CTL, and XJD, average drought severity calculated from of SPI-3 series (Fig. 7(a)) was larger than that calculated from of SRI-3 series (Fig. 7(c)). The largest drought severity were in the CTL (10.38) and XQ (9.20) catchments for SPI-3 and SRI-3, respectively. For the disturbed period, however, drought severity was larger for hydrological drought (Fig. 7(d)) than meteorological drought (Fig. 7(b)) across all human-impacted catchments in the Laohahe basin. For example, the average drought severity calculated from SRI-3 in disturbed period was 13.1 in the XLP catchment, but that calculated from SPI-3 in the same catchment was only 2.2, with a six-fold difference between the two values.

Insert Figure 7 about here

Furthermore, Table 6 shows the difference in average drought characteristics calculated from SPI-3 and SRI-3 series between undisturbed and disturbed periods for all catchments. Meteorological drought measured by SPI-3 had no significant change between undisturbed and disturbed periods for all catchments. Differences in the average meteorological drought duration and severity between the two periods were 0.8% and 0.5% for natural catchments, 2.1% and 8.9% for human-impacted catchments (I), and 2.6% and 7.8% for human-impacted catchments (II) respectively. However, for hydrological drought, the average drought duration and severity during the disturbed period were significant higher than those during the undisturbed period. In particular, increases of 114.6% and 110.7% for drought duration and severity in human-impacted catchments (I), and 193.2% and 518.8% for those in human-impacted catchments (II), were higher than those for natural catchments, i.e., 47.4% and 43.8%. Therefore, hydrological drought of human-impacted catchments in the Laohahe basin was influenced not only by climate change (e.g., precipitation and temperature) but also by human activities (e.g., human water withdrawal, reservoir regulations, and land use and cover change).

Insert Table 6 about here

4.2.3 Propagation from meteorological to hydrological drought

To investigate the most appropriate accumulation period for propagation time from meteorological to hydrological drought, the SRI-1 series was cross-correlated with the SPI series at various timescales (spanning 1–48 months) (Fig. 8). All the catchments were divided into three groups according to catchment area to avoid its impact on drought propagation (as shown in Table 5). The first and second groups include the three natural catchments, i.e., YSWZ, JS, and XQ catchments (Fig. 8(a) and (d)), and three human-impacted catchments, i.e., XJD, XCZ, and DZ catchments (Fig. 8(b) and (e)), because all their catchment area are less than 2000 km^2. Remain catchments are classed into the third group (Fig. 8(c) and (f)) because all their catchments are greater than 2000 km^2. The PCC for natural catchments during the undisturbed period (Fig. 8(a)) increased rapidly and reached the maximum value in the range of 11–15 months. The highest PCCs for the YSWZ, JS, and XQ catchments were 0.72, 0.75, and 0.70, respectively, and the corresponding propagation times were 12, 12, and 14 months, respectively. For human-impacted catchments (I) during the undisturbed period, XCZ, DZ, and XJD catchments reached the maximum PCC value in the range of 6–13 months (Fig. 8(b)), and the maximum PCC values for human-impacted catchments (II) were concentrated in the range of 8–13 months (Fig. 8(c)), with the highest PCC varying from 0.36 to 0.59. In the disturbed period, the most appropriate accumulation periods for drought propagation time in natural catchments concentrated in the range of 7–12 months (Fig. 8(d)). For the human-impacted catchments, the PCC values of the XCZ, DZ, and XJD catchments reached the maximum value in the range of 9–13 months (Fig. 8(e)), while remain catchments reached the highest PCC values in the range of 17–24 months (Fig. 8(f)).

Insert Figure 8 about here

In addition, Fig. 9 shows the seasonal variability in the drought propagation time and the corresponding strongest PCC values during undisturbed and disturbed periods. For natural catchments (i.e., YSWZ, JS, and XQ), propagation times in spring (March–May) and summer (June–August) during undisturbed times were relatively consistent with those during the disturbed period. However, the propagation times in autumn (September–November) and winter (December–February) during the disturbed period were shorter than those during the undisturbed period, which result in that the drought propagation time during the disturbed period is shorter than that in the undisturbed period. For human-impacted catchments (i.e., the remaining eight catchments), except in summer, propagation times in the other three seasons were longer for the disturbed period than for the undisturbed period. Therefore, increases in propagation times during disturbed period for human-impacted catchments were mainly concentrated in spring, autumn, and winter.

Insert Figure 9 about here

4.3 Impact of climate change and human activities on drought propagation

In this study, we designed three comparisons to reveal the impacts of climate change and human activities on drought propagation from meteorological to hydrological drought (Fig. 2 and Table 7). First of all, we compared the propagation time of natural and human-impacted catchments during the undisturbed period in comparison Ⅰ, the differences between natural and human-impacted (I) catchments for the mean, median, and maximum drought propagation time are 3, 3, and 2 months respectively, and the above differences between natural and human-impacted (II) catchments are 2, 1, and 2 months respectively, indicating that drought propagation patterns of all catchments in Laohahe basin are generally consistent. Then, the drought propagation time of natural catchments between the undisturbed and disturbed periods was compared in comparison Ⅱ to reflect the influence of climate change on drought propagation. The results revealed that the average, median and maximum drought propagation times in the natural catchments during the disturbed period were reduced by approximately 3 months, indicating that drought propagation is accelerating under the influence of climate change. Finally, in comparison Ⅲ, the propagation time of human-impacted catchments was compared with those of natural catchments during the disturbed period. The former was influenced by climate change and human activities, and the latter was influenced by climate change only. Difference between them can reveal the impacts of human activities on the drought propagation process. The mean, median, and maximum values of the propagation time for human-impacted (I) catchments increased by approximately 2, 2, and 1 months, respectively, and the above increase for human-impacted (II) catchments are 12, 11, and 12 months, indicating that human activities significantly disturb and delay natural drought propagation processes of the midstream and downstream catchments (i.e., XD, CF, TPZ, and XLP catchments) during disturbed periods.

Insert Table 7 about here

5. Discussion

5.1 Rationality analysis of the natural and human-impacted catchment comparison method

Under the background of global change, we need to improve our understanding of the impacts of different factors on drought propagation. These processes can be deeply explored through observation-based data. In this study, we proposed the natural and human-impacted catchment comparison method, which selects natural catchments though analysis of hydrological variations, as well as statistics analysis of human influence based on an indicator system. More importantly, it used only observation data to analyse the impacts of climate change and human activities on drought propagation, which can improve the accuracy of the impact assessment.

On the one hand, the selection results of natural catchments in the Laohahe basin were consistent with previous studies. Yong et al. (2013) found that the YSWZ and JS catchments had no significant change points in runoff based on the Pettitt test and DCC method. Wang et al. (2020) selected the XQ catchment as a natural catchment to analyse the uncertainty of hydrological models because it has a consistent relationship between precipitation and runoff. Therefore, the natural catchments selected in this study, including the YSWZ, JS, and XQ catchments, were reasonable.

On the other hand, the analysis of the impacts of climate change and human activities on drought propagation in this study were also consistent with other studies

(Jiang et al., 2019; Liu et al., 2016; Barker et al., 2016; López-Moreno et al., 2013; Liu et al., 2009). Han et al. (2019) pointed out that the phase transformation and amplitude fluctuation of PDO and ENSO are obviously enhanced in the 21st century, which intensifies the changes in meteorological elements such as temperature, precipitation and evaporation and then accelerates the propagation time from meteorological drought to hydrological drought. For human influence, Lorenzo-Lacruz et al. (2013) stated that human activities have significantly altered the natural hydrological response (e.g., hydrological drought) to meteorological droughts, delaying the response of hydrological drought to precipitation deficits over long timescales. Thus, the results obtained by the proposed method are consistent with previous studies, i.e., climate change tends to accelerate drought propagation, and human influence tends to delay drought propagation in the Laohahe basin.

Furthermore, the proposed method provides a new idea for the selection of natural catchments, i.e., using an indicator system that involving socio-economic indices to quantify human influence, and combining its results with hydrological variation results to support catchment division. With the increasing development of earth observation technology, a large number of remote sensing inversion and reanalysis data sets have appeared (Tapley et al., 2004; Theobald et al., 2010; Small et al., 2011; Ma et al., 2012; Yue et al., 2014; Perkl et al., 2016; Sheffield et al., 2017). These data sets provide new reference indicators, that is, socio-economic attributes (e.g. population and GDP density, and land use situation) for catchment division, in addition to the traditional hydrological attributes. Therefore, when it is difficult to use exciting methods to select natural catchments, the proposed method may be a good supplement or choice. For example, when we cannot find suitable paired catchments using the paired-catchments comparison method, or want to remove the concern of variations across paired catchments, the proposed method can be used to determine natural and human-impacted catchments.

More importantly, different comparison schemes in the proposed method can identify the changes of drought propagation process in different types of catchments (natural or human-impacted catchment), which are equally important for water resource managers. For natural catchments, understanding the changes of drought propagation due to climate change is helpful to the improvement of drought prediction (Huang et al., 2017; Han et al., 2019; AghaKouchak et al., 2021). For human-impacted catchments, realizing that changes of drought propagation pattern caused by human influence is important for water resource managers to adjust water resources allocation to cope with the possible water supply crisis and ecological crisis caused by the above changes (Van Loon et al., 2016; Apurv and Cai, 2020; AghaKouchak et al., 2021).

In general, the case study results in Laohahe basin proved that the proposed method is an effective tool for selection of natural catchments and assessing climatic and anthropogenic influences on drought propagation, and can be applied to other regions as well to improve drought prediction and regional water resources management.

5.2 Possible factors influencing drought propagation

5.2.1 Influence of teleconnection factors on drought propagation

In comparison II (as shown in Fig. 2 and Table 7), the results showed that climate change accelerates the drought propagation in natural catchment. And recent studies have found that large-scale atmospheric circulation anomalies, which are closely related to climate change, may have impacts on the drought propagation time (Huang et al., 2017). Meanwhile, evaporation plays an important role in the drought propagation process from meteorological to hydrological drought (Han et al., 2019). Thus, wavelet cross-analysis was applied to analyse the correlations between the actual evaporation in a natural catchment, i.e., JS catchment, and teleconnection factors, i.e., ENSO, AO, PDO, and sunspots series during 1964–2016 (Fig. 10). The results showed that actual evaporation had significant positive linkages with ENSO events (Fig. 10(a)) with periods of 3–7 years during 1985–2005 and PDO events (Fig. 10(c)) with periods of 4–7 years and 8–12 years during 1990-2000 at the 95% confidence level. Moreover, actual evaporation had strong negative correlations with AO, and sunspots. Specifically, it exhibited a negative correlation with AO with periods of 8–10 years during 1980–1995, and a strong negative correlation with sunspots, with periods of 7–14 years during

1973–2005. Therefore, large-scale atmospheric circulation anomalies show strong linkages with actual evaporation during the disturbed period (1980-2016), thus strongly affecting the propagation time from meteorological to hydrological drought in this period. These findings are similar to those from other studies (Huang et al., 2017; Han et al., 2019), and closely related to the changes of drought propagation time in natural catchments during the disturbed period.

Insert Figure 10 about here

5.2.2 Impact of human factors on drought propagation

In the comparison III (as shown in Fig. 2 and Table 7), the results showed that human activities, including economic development, reservoir construction, and land use and cover change, significantly altered and then delayed the drought propagation time. Firstly, population and economic development have significant impacts on drought propagation. As shown in Fig. 4(a)-(c), population density of the two highly industrialized human-impacted catchments, i.e., CF and XLP catchments reached approximately 200 persons/km^2, and GDP and night light density of these two catchments increased rapidly after 2000. More intuitively, Fig. 11(a) shows that in 2006-2016, the total annual human water withdrawal of the human-impacted catchments account for more than half of the natural runoff for the Laohahe basin, and the highest proportion is approximately 80%. Except for the XJD catchment, all the human-impacted catchments were directly impacted by human water withdrawal. Thus, sustained increase of domestic water and industrial water for economic development causes serious loss of surface water and then extends the response times of hydrological drought to meteorological drought.

Reservoir constructions and regulations might be another factor affecting drought propagation. For example, the Dahushi reservoir, located in DZ catchment with a storage capacity of 1.2×10^8 m^3, focused on agricultural irrigation and usually maintained storage in spring, autumn, and winter, and then released water in summer to guarantee agriculture irrigation (Yong et al., 2013; Ren et al., 2014; Jiang et al., 2021). These seasonal regulations are closely related to the shifts of seasonal pattern of drought propagation. As shown in Fig. 9, except for summer (June, July, and August), drought propagation time of the other seasons in human-impacted catchments (e.g., CTL, XD, CF, TPZ, and XLP) become longer for disturbed period than for undisturbed period, indicating that reservoir regulations modifies the response pattern of hydrological drought to meteorological drought in different seasons and tends to smooth the impacts of meteorological drought over a longer time scale.

In addition to economic development and reservoir regulations, land use change and intensification of agriculture activities may also impacted drought propagation. As shown in Fig. 4(d), compared with the three natural catchments (i.e., YSWZ, XQ, and JS), remain eight human-impacted catchments have a higher proportion of cropland and urban land, especially the midstream and downstream catchment (e.g., CF, TPZ, and XLP catchments). The proportion of cropland and urban land for the TPZ catchment increased from 55% in 1980 to 60% in 2015, and that for CF catchment increased from 46% in 1980 to 50% in 2015. In addition, Fig. 11(b) shows that agriculture production data including irrigated area, livestock, and food production and the GIP have a substantial increase during the disturbed period (1980-2016), and Fig. 11(c) shows that surface soil moisture increases significantly after 2000, which is closely related to the large-scale intensive agricultural irrigation activities. Thus, increase of area of cropland and intensification of agriculture production activities consume a large amount of surface water, leading to a sharp decrease in river runoff, which in turn delays the propagation from meteorological to hydrological drought.

Finally, terrestrial water storage anomaly (TWSA) data were used to reveal the changes in total water resources in the Laohahe basin (Fig. 11(d)). Water storage in the Laohahe basin declined significantly during 2003–2016, especially after 2007 (–0.63 cm/a), and the largest negative anomaly reached approximately 16 cm/year (approximately equal to 6 times the average annual runoff of the Laohahe basin). In general, human activities such as socio-economic development (e.g. population, GDP, and night light density), reservoir constructions and regulations, and land use change, have significantly modified the total amount and temporal distribution of the surface runoff in the Laohahe basin, which in turn lead a delayed and more sustained response of hydrological drought to meteorological drought.

Insert Figure 11 about here

5.3 Uncertainties and limitations

The results demonstrated that the proposed method is a suitable tool to analyse the impacts of climate change and human activities on drought propagation. However, this approach still has some uncertainties. Most observation-based methods have uncertainties with regard to temporal or spatial resolution and data quality (Rangecroft et al., 2019). Limitations in the accuracy of hydrometric gauges (particularly during low flows) and the evolution of hydrological stations over time mean that it is often difficult to have an accurate, homogeneous flow record (Margariti et al., 2019), which creates uncertainty and then influences the calculation accuracy of meteorological and hydrological droughts. However, it has been recognized that the benefit of using these longer records for our analysis outweighs the disadvantages of uncertain hydrometric accuracy.

Besides, many previous studies have proven that the drought propagation time is closely linked with climate and catchment properties (e.g., land use and soil types) (Barker et al., 2016; Van Loon and Laaha, 2015). Even if the selected natural catchments and human-impacted catchments are distributed in the same basin, differences in climate and catchment properties still bring some uncertainties to the comparison results. Nevertheless, comparison Ⅰ (Fig. 2) in the proposed method is used to assess the similarity of drought propagation pattern in different sub-catchments. Comparison results (Fig. 8(a)-(c)) indicated that, in the undisturbed period, the drought propagation time of natural catchments is close to that of human-impacted catchments, which means that differences in climate and catchment properties for the selected catchments did not cause significant differences in the drought propagation time.

Meanwhile, it is worth noting that directly comparing the drought propagation characteristics of the two periods before and after the change point in natural catchments to quantify the impacts of climate change may also bring uncertainties. Because climate change is a gradual changing process, its impact on drought propagation may continuously increase since the beginning of the study period. Stochastic weather generator (Semenov, 2008; Wilks and Wilby, 1999) will be a good choice to solve the gradually changing weather patterns for its strong advantage of generating long time series of weather variables with statistical properties identical to those of observed series (Sohrabi et al., 2021). In future research, we can use the stochastic weather generator to simulate the weather variables in the disturbed period (the period after the change point) based on the those in the undisturbed period (the period before the change point), so as to ensure that the statistical characteristics of the two series are the same. Then, the corresponding drought propagation characteristics under the observed and simulated weather conditions in the disturbed period can be compared to quantify the impacts of climate change in this period.

In addition to the uncertainty, there are some limitations to this approach. Firstly, this method needs specific and numerous data to divide natural and human-impacted catchments. Long time series of hydrological data are needed to identify whether there are change points in hydrological processes. More specific land use data and socio-economic indicators based on remote sensing inversion and reanalysis (i.e., GDP, population, and night light density) are needed to quantify human influence to support for the selection of natural catchments. However, the above data are not always available or known (Van Loon et al., 2019; Wang et al., 2020). Moreover, because monthly data (e.g., precipitation and streamflow) were used, the baseflow separation is not considered in this study, which will also affect the study results. So we suggest when using the proposed approach in other regions, it is necessary to separate runoff from baseflow based on data with shorter time scale (e.g., daily data) to ensure the accuracy of the results.

Secondly, it remains difficult to select natural catchments using this indicator system for catchment with more complex situation. Thus, other indicators representing human activities can be developed in future studies and then appropriately applied to the index system, so as to provide a more accurate selection (Li et al., 2020). Meanwhile, there is another challenge, i.e., how to comprehensively consider various types of indicators to characterize the influence of human activities and apply them in the selection of natural catchments. Because subjective choices might lead to the deviation of the selection results (Sanderson et al., 2002; Woolmer et al., 2008). In this study, different indicators were scored based on the existing researches (as shown in Table 3), and then the catchments were divided according to the results of HI and hydrological variation analysis. In the future research, more case studies on the indicator system are needed to make the division criteria (e.g., threshold of HI) more reasonable and objective.

In view of the benefits and limitations, we suggest that when using this method in other regions, the selection of socio-economic indicators and setting of threshold of HI should be modified and improved appropriately according to specific situation of the catchment itself and the types of human activities. Furthermore, the approach can be used for a first estimate of the human influence, to guide campaigns to collect more data, and to complement other existing methods (e.g. large-scale screening, paired catchments, and observation-modelling approaches).

6. Conclusions

In this study, we proposed an observation-based natural and human-impacted catchment comparison method for separating the effects of climate change and human activities on drought propagation. The main parts of this method are the selection of natural catchments and the comparison of natural and human-impacted situations in different periods. First, observed data, i.e., hydro-meteorological data, as well as land use data and socio-economic indicators based on remote sensing inversion and reanalysis, are used to select natural catchments. Then, three comparisons can be performed to separate the effects of climate change and human activities on drought propagation, i.e., comparison Ⅰ during the undisturbed period to analyse the consistency of drought propagation pattern in natural and human-impacted catchments, comparison Ⅱ between the disturbed and undisturbed periods to identify the possible influence of climate change, and comparison Ⅲ during the disturbed period to investigate human impacts. The combination of these three comparison schemes to separate the effects of climate change and human activities on drought propagation is the innovative part of this research.

We demonstrate the application of the proposed natural and human-impacted catchment comparison method in a heavily human-influenced basin in northeast China, i.e., the Laohahe basin. In this basin, we found that human activities caused longer hydrological drought durations and larger hydrological drought severities during the disturbed period, with average increases of 163.7% and 365.9%, respectively. Furthermore, comparison results revealed that climate change accelerated the propagation from meteorological to hydrological drought in the Laohahe basin, shortening it by approximately 3 months. Human activities, however, disturbed and then delayed the natural propagation from meteorological to hydrological drought, extending it by 11–12 months.

The proposed natural and human-impacted catchment comparison method gives water managers a suitable tool to divide natural and human-impacted catchments based on hydrological and socio-economic data and then to investigate how climatic and anthropogenic influences alter drought propagation through different comparison schemes. This is critical for improving drought prediction and establishing a drought management system.

Acknowledgments

This work was financially supported by the National Key Research and Development Program approved by Ministry of Science and Technology, China (2016YFA0601500; 2018YFC0407704); the National Natural Science Foundation of China (51979069; 51879163); the Fundamental Research Funds for the Central Universities (B200204029); the Programme of Introducing Talents of Discipline to Universities by the Ministry of Education and the State Administration of Foreign Experts Affairs, China (B08048); the National Natural Science Foundation of Jiangsu Province, China (BK20180512).

References

AghaKouchak, A., Feldman, D., Hoerling, M., Huxman, T., Lund, J., 2015. Water and climate: Recognize anthropogenic drought. Nature 524, 409–411. https://doi.org/10.1038/524409a

AghaKouchak, A., Mirchi, A., Madani, K., Di Baldassarre, G., Nazemi, A., Alborzi, A., Anjileli, H., Azarderakhsh, M., Chiang, F., Hassanzadeh, E., Huning, L.S., Mallakpour, I., Martinez, A., Mazdiyasni, O., Moftakhari, H., Norouzi, H., Sadegh, M., Sadeqi, D., Van Loon, A.F., Wanders, N., 2021. Anthropogenic Drought:

Definition, Challenges, and Opportunities. Rev. Geophys. 59, 1–23. https://doi.org/10.1029/2019rg000683

Allen, R.G., Pereira, L.S., Raes, D., et al., 1998. Crop Evapotranspiration Guidelines for Computing Crop Water Requirements. FAO Irrigation and Drainage Paper No. 56. FAO, Rome.

Apurv, T., Cai, X., 2020. Drought Propagation in Contiguous U.S. Watersheds: A Process-Based Understanding of the Role of Climate and Watershed Properties. Water Resour. Res. 56, 1–23. https://doi.org/10.1029/2020WR027755

Barker, L.J., Hannaford, J., Chiverton, A., Svensson, C., 2016. From meteorological to hydrological drought using standardised indicators. Hydrol. Earth Syst. Sci. 20, 2483–2505. https://doi.org/10.5194/hess-20-2483-2016

Bernaola-Galván, P., Ivanov, P.C., Nunes Amaral, L.A., Stanley, H.E., 2001. Scale invariance in the nonstationarity of human heart rate. Phys. Rev. Lett. 87, 1–4. https://doi.org/10.1103/PhysRevLett.87.168105

Chen, Y., Feng, X., Fu, B., 2021. An improved global remote-sensing-based surface soil moisture (RSSSM) dataset covering 2003--2018. Earth Syst. Sci. Data 13, 1–31. https://doi.org/10.5194/essd-13-1-2021

Dai, A., 2011. Drought under global warming: A review. Wiley Interdiscip. Rev. Clim. Chang. 2, 45–65. https://doi.org/10.1002/wcc.81

Eltahir, E.A.B., Yeh, P.J.F., 1999. On the asymmetric response of aquifer water level to floods and droughts in Illinois. Water Resour. Res. 35, 1199–1217. https://doi.org/10.1029/1998WR900071

Farahmand, A., AghaKouchak, A., 2015. A generalized framework for deriving nonparametric standardized drought indicators. Adv. Water Resour. 76, 140–145. https://doi.org/10.1016/j.advwatres.2014.11.012

Ficklin, D.L., Abatzoglou, J.T., Robeson, S.M., Null, S.E., Knouft, J.H., 2018. Natural and managed watersheds show similar responses to recent climate change. Proc. Natl. Acad. Sci. U. S. A. 115, 8553–8557. https://doi.org/10.1073/pnas.1801026115

Grinsted, A., Moore, J.C., Jevrejeva, S., 2004. Application of the cross wavelet transform and wavelet coherence to geophysical time series. Nonlinear Process. Geophys. 11, 561–566. https://doi.org/10.5194/npg-11-561-2004

Hamed, K.H., Ramachandra Rao, A., 1998. A modified Mann-Kendall trend test for autocorrelated data. J. Hydrol. 204, 182–196. https://doi.org/10.1016/S0022-1694(97)00125-X

Han, X.D.; Zhou, Y.; Wang, S.X.; Liu, R.; Yao, Y., 2012. GDP spatialization in China based on DMSP/OLS data and land use data. Remote Sens. Technol. Appl. 27(3), 396–405.

Han, Z., Huang, S., Huang, Q., Leng, G., Wang, H., Bai, Q., Zhao, J., Ma, L., Wang, L., Du, M., 2019. Propagation dynamics from meteorological to groundwater drought and their possible influence factors. J. Hydrol. 578, 124102. https://doi.org/10.1016/j.jhydrol.2019.124102

Heudorfer, B., Stahl, K., 2017. Comparison of different threshold level methods for drought propagation analysis in Germany. Hydrol. Res. 48, 1311–1326. https://doi.org/10.2166/nh.2016.258

Huang, S., Huang, Q., Chang, J., Zhu, Y., Leng, G., Xing, L., 2015. Drought structure based on a nonparametric multivariate standardized drought index across the Yellow River basin, China. J. Hydrol. 530, 127–136. https://doi.org/10.1016/j.jhydrol.2015.09.042

Huang, S., Li, P., Huang, Q., Leng, G., Hou, B., Ma, L., 2017. The propagation from meteorological to hydrological drought and its potential influence factors. J. Hydrol. 547, 184–195. https://doi.org/10.1016/j.jhydrol.2017.01.041

Hudgins, L., Huang, J., 1996. Bivariate Wavelet Analysis of Asia Monsoon and ENSO. Adv. Atmos. Sci. 13, 299–312. https://doi.org/10.1007/BF02656848

Jiang, S., Ren, L., Yong, B., Singh, V.P., Yang, X., Yuan, F., 2011. Quantifying the effects of climate variability and human activities on runoff from the Laohahe basin in northern China using three different methods. Hydrol. Process. 25, 2492–2505. https://doi.org/10.1002/hyp.8002

Jiang, S., Wang, M., Ren, L., Xu, C.Y., Yuan, F., Liu, Y., Lu, Y., Shen, H., 2019. A framework for quantifying the impacts of climate change and human activities on hydrological drought in a semiarid basin of Northern China. Hydrol. Process. 33, 1075–1088. https://doi.org/10.1002/hyp.13386

Jiang, S., Zhou, L., Ren, L., Wang, M., Xu, C.Y., Yuan, F., Liu, Y., Yang, X., Ding, Y., 2021. Development of a comprehensive framework for quantifying the impacts of climate change and human activities on river hydrological health variation. J. Hydrol. 600, 126566. https://doi.org/10.1016/j.jhydrol.2021.126566

Konapala, G., Mishra, A., 2020. Quantifying climate and catchment control on hydrological drought in the continental United States. Water Resour. Res. 56. https://doi.org/10.1029/2018WR024620

Li, Q., Zhou, J., Zou, W., Zhao, X., Huang, P., Wang, L., Shi, W., Ma, X., Zhao, Y., Xue, D., Dou, J., Wei, W., Zhu, G., 2020. A tributary-comparison method to quantify the human influence on hydrological drought. J. Hydrol. 125652. https://doi.org/10.1016/j.jhydrol.2020.125652

Liu, X., Ren, L., Yuan, F., Singh, V.P., Fang, X., Yu, Z., Zhang, W., 2009. Quantifying the effect of land use and land cover changes on green water and blue water in northern part of China. Hydrol. Earth Syst. Sci. 13, 735–747. https://doi.org/10.5194/hess-13-735-2009

Liu, Y., Ren, L., Zhu, Y., Yang, X., Yuan, F., Jiang, S., Ma, M., 2016. Evolution of Hydrological Drought in Human Disturbed Areas: A Case Study in the Laohahe Catchment, Northern China. Adv. Meteorol. 2016. https://doi.org/10.1155/2016/5102568

López-Moreno, J.I., Vicente-Serrano, S.M., Zabalza, J., Beguería, S., Lorenzo-Lacruz, J., Azorin-Molina, C., Morán-Tejeda, E., 2013. Hydrological response to climate variability at different time scales: A study in the Ebro basin. J. Hydrol. 477, 175–188. https://doi.org/10.1016/j.jhydrol.2012.11.028

Lorenzo-Lacruz, J., Vicente-Serrano, S.M., González-Hidalgo, J.C., López-Moreno, J.I., Cortesi, N., 2013. Hydrological drought response to meteorological drought in the Iberian Peninsula. Clim. Res. 58, 117–131. https://doi.org/10.3354/cr01177

Longobardi, A., & Van Loon, A. F., 2018. Assessing baseflow index vulnerability to variation in dry spell length for a range of catchment and climate properties. Hydrological Processes, 32(16), 2496–2509. https://doi.org/10.1002/hyp.13147

Ma, T., Zhou, C., Pei, T., Haynie, S., Fan, J., 2012. Quantitative estimation of urbanization dynamics using time series of DMSP/OLS nighttime light data: A comparative case study from China’s cities. Remote Sens. Environ. 124, 99–107. https://doi.org/10.1016/j.rse.2012.04.018

Margariti, J., Rangecroft, S., Parry, S., Wendt, D.E., Van Loon, A.F., 2019. Anthropogenic activities alter drought termination. Elementa 7. https://doi.org/10.1525/elementa.365

Mishra, A.K., Singh, V.P., 2010. A review of drought concepts. J. Hydrol. 391, 202–216. https://doi.org/10.1016/j.jhydrol.2010.07.012

Pearson, K. (1895). Notes on regression and inheritance in the case of two parents. Proceedings of the Royal Society of London, 58(1), 240–242. https://doi.org/10.1098/rspl.1895.0041

Peñas, F.J., Barquín, J., Álvarez, C., 2016. Assessing hydrologic alteration: Evaluation of different alternatives according to data availability. Ecol. Indic. 60, 470–482. https://doi.org/10.1016/j.ecolind.2015.07.021

Perkl, R.M., 2016. Measuring landscape integrity (LI): development of a hybrid methodology for planning applications. J. Environ. Plan. Manag. 60, 92–114. https://doi.org/10.1080/09640568.2016.1142863

Peters, E., Torfs, P.J.J.F., Van Lanen, H.A.J., Bier, G., 2003. Propagation of drought through groundwater - A new approach using linear reservoir theory. Hydrol. Process. 17, 3023–3040. https://doi.org/10.1002/hyp.1274

Pettitt, 1979. A Non-parametric to the Approach Problem. Appl. Stat. 28, 126–135.

Rangecroft, S., Van Loon, A.F., Maureira, H., Verbist, K., Hannah, D.M., 2019. An observation-based method to quantify the human influence on hydrological drought: upstream–downstream comparison. Hydrol. Sci. J. 64, 276–287. https://doi.org/10.1080/02626667.2019.1581365

Ren, L., Yuan, F., Yong, B., Jiang, S., Yang, X., Gong, L., Ma, M., Liu, Y., Shen, H., 2014. Where does blue water go in the semi-arid area of northern China under changing environments? Proc. IAHS, 364, 88–93.

Roodari, A., Hrachowitz, M., Hassanpour, F., Yaghoobzadeh, M., 2021. Signatures of human intervention-or not? Downstream intensification of hydrological drought along a large Central Asian river: The individual roles of climate variability and land use change. Hydrol. Earth Syst. Sci. 25, 1943–1967. https://doi.org/10.5194/hess-25-1943-2021

Sanderson, E.W., Jaiteh, M., Levy, M.A., Redford, K.H., Wannebo, A. V., Woolmer, G., 2002. The human footprint and the last of the wild. Bioscience 52, 891–904. https://doi.org/10.1641/0006-3568(2002)052[0891:THFATL]2.0.CO;2

Semenov, M.A., 2008. Simulation of extreme weather events by a stochastic weather generator. Clim. Res. 35, 203–212. https://doi.org/10.3354/cr00731

Sheffield, J., Wood, E.F., Roderick, M.L., 2012. Little change in global drought over the past 60 years. Nature 491, 435–438. https://doi.org/10.1038/nature11575

Sheffield, J., Wood, E.F., Pan, M., Beck, H., Coccia, G., Serrat-Capdevila, A., Verbist, K., 2018. Satellite Remote Sensing for Water Resources Management: Potential for Supporting Sustainable Development in Data-Poor Regions. Water Resour. Res. 54, 9724–9758. https://doi.org/10.1029/2017WR022437

Shukla, S., Wood, A.W., 2008. Use of a standardized runoff index for characterizing hydrologic drought. Geophys. Res. Lett. 35, 1–7. https://doi.org/10.1029/2007GL032487

Small, C., Elvidge, C.D., Balk, D., Montgomery, M., 2011. Spatial scaling of stable night lights. Remote Sens. Environ. 115, 269–280. https://doi.org/10.1016/j.rse.2010.08.021

Sohrabi, S., Brissette, F.P., Arsenault, R., 2021. Coupling large-scale climate indices with a stochastic weather generator to improve long-term streamflow forecasts in a Canadian watershed. J. Hydrol. 594, 125925. https://doi.org/10.1016/j.jhydrol.2020.125925

Stephens, C.M., Lall, U., Johnson, F.M., Marshall, L.A., 2021. Landscape changes and their hydrologic effects: Interactions and feedbacks across scales. Earth-Science Rev. 212, 103466. https://doi.org/10.1016/j.earscirev.2020.103466

Tallaksen, L.M., Hisdal, H., Lanen, H.A.J.V., 2009. Space-time modelling of catchment scale drought characteristics. J. Hydrol. 375, 363–372. https://doi.org/10.1016/j.jhydrol.2009.06.032

Tapley, B.D., Bettadpur, S., Ries, J.C., Thompson, P.F., Watkins, M.M., 2004. GRACE measurements of mass variability in the Earth system. Science. 305, 503–505. https://doi.org/10.1126/science.1099192

Theobald, D.M., 2010. Estimating natural landscape changes from 1992 to 2030 in the conterminous US. Landsc. Ecol. 25, 999–1011. https://doi.org/10.1007/s10980-010-9484-z

Tijdeman, E., Menzel, L., 2020. Controls on the development and persistence of soil moisture drought across Southwestern Germany. Hydrol. Earth Syst. Sci. (in press) 1–20. https://doi.org/10.5194/hess-2020-307

Tijdeman, E., Barker, L.J., Svoboda, M.D., Stahl, K., 2018. Natural and Human Influences on the Link Between Meteorological and Hydrological Drought Indices for a Large Set of Catchments in the Contiguous United States. Water Resour. Res. 54, 6005–6023. https://doi.org/10.1029/2017WR022412

Torrence, C., Compo, G.P., 1998. A Practical Guide to Wavelet Analysis. Bull. Am. Meteorol. Soc. 79, 61–78. https://doi.org/10.1175/1520-0477(1998)079<0061:APGTWA>2.0.CO;2

Van Lanen, H.A.J., Wanders, N., Tallaksen, L.M., Van Loon, A.F., 2013. Hydrological drought across the world: Impact of climate and physical catchment structure. Hydrol. Earth Syst. Sci. 17, 1715–1732. https://doi.org/10.5194/hess-17-1715-2013

Van Loon, A.F., Laaha, G., 2015. Hydrological drought severity explained by climate and catchment characteristics. J. Hydrol. 526, 3–14. https://doi.org/10.1016/j.jhydrol.2014.10.059

Van Loon, A.F., Van Lanen, H.A.J., 2013. Making the distinction between water scarcity and drought using an observation-modeling framework. Water Resour. Res. 49, 1483–1502. https://doi.org/10.1002/wrcr.20147

Van Loon, A.F., Van Lanen, H.A.J., 2012. A process-based typology of hydrological drought. Hydrol. Earth Syst. Sci. 16, 1915–1946. https://doi.org/10.5194/hess-16-1915-2012

Van Loon, A.F., 2015. Hydrological drought explained. Wiley Interdiscip. Rev. Water 2, 359–392. https://doi.org/10.1002/wat2.1085

Van Loon, A.F., Gleeson, T., Clark, J., Van Dijk, A.I.J.M., Stahl, K., Hannaford, J., Di Baldassarre, G., Teuling, A.J., Tallaksen, L.M., Uijlenhoet, R., Hannah, D.M., Sheffield, J., Svoboda, M., Verbeiren, B., Wagener, T., Rangecroft, S., Wanders, N., Van Lanen, H.A.J., 2016. Drought in the Anthropocene. Nat. Geosci. 9, 89–91. https://doi.org/10.1038/ngeo2646

Van Loon, A.F., Rangecroft, S., Coxon, G., Naranjo, J.A.B., Van Ogtrop, F., Van Lanen, H.A.J., 2019. Using paired catchments to quantify the human influence on hydrological droughts. Hydrol. Earth Syst. Sci. 23, 1725–1739. https://doi.org/10.5194/hess-23-1725-2019

Veettil, A.V., Konapala, G., Mishra, A.K., Li, H.Y., 2018. Sensitivity of drought resilience-vulnerability- exposure to hydrologic ratios in contiguous United States. J. Hydrol. 564, 294–306. https://doi.org/10.1016/j.jhydrol.2018.07.015

Veettil, A.V., Mishra, A. k., 2020. Multiscale hydrological drought analysis: Role of climate, catchment and morphological variables and associated thresholds. J. Hydrol. 582, 124533. https://doi.org/10.1016/j.jhydrol.2019.124533

Vicente-Serrano, S.M., López-Moreno, J.I., Beguería, S., Lorenzo-Lacruz, J., Azorin-Molina, C., Morán-Tejeda, E., 2012. Accurate Computation of a Streamflow Drought Index. J. Hydrol. Eng. 17, 318–332. https://doi.org/10.1061/(asce)he.1943-5584.0000433

Vidal, J.P., Martin, E., Franchistéguy, L., Habets, F., Soubeyroux, J.M., Blanchard, M., Baillon, M., 2010. Multilevel and multiscale drought reanalysis over France with the Safran-Isba-Modcou hydrometeorological suite. Hydrol. Earth Syst. Sci. 14, 459–478. https://doi.org/10.5194/hess-14-459-2010

Wagener, T., Sivapalan, M., Troch, P.A., McGlynn, B.L., Harman, C.J., Gupta, H. V., Kumar, P., Rao, P.S.C., Basu, N.B., Wilson, J.S., 2010. The future of hydrology: An evolving science for a changing world. Water Resour. Res. 46, 1–10. https://doi.org/10.1029/2009WR008906

Wang, M., Jiang, S., Ren, L., Xu, C.Y., Yuan, F., Liu, Y., Yang, X., 2020. An approach for identification and quantification of hydrological drought termination characteristics of natural and human-impacted series. J. Hydrol. 590. https://doi.org/10.1016/j.jhydrol.2020.125384

Wei, L., Jiang, S., Ren, L., Tan, H., Ta, W., Liu, Y., Yang, X., Zhang, L., Duan, Z., 2021. Spatiotemporal changes of terrestrial water storage and possible causes in the closed Qaidam Basin, China using GRACE and GRACE Follow-On data. J. Hydrol. 598, 126274. https://doi.org/10.1016/j.jhydrol.2021.126274

Wells, N., Goddard, S., Hayes, M.J., 2004. A self-calibrating Palmer Drought Severity Index. J. Clim. 17, 2335–2351. https://doi.org/10.1175/1520-0442(2004)017<2335:ASPDSI>2.0.CO;2

Wilks, D.S., Wilby, R.L., 1999. The weather generation game: a review of stochastic weather models. Prog. Phys. Geogr. 23, 329–357.

Woolmer, G., Trombulak, S.C., Ray, J.C., Doran, P.J., Anderson, M.G., Baldwin, R.F., Morgan, A., Sanderson, E.W., 2008. Rescaling the Human Footprint: A tool for conservation planning at an ecoregional scale. Landsc. Urban Plan. 87, 42–53. https://doi.org/10.1016/j.landurbplan.2008.04.005

Wu, J., Miao, C., Zheng, H., Duan, Q., Lei, X., Li, H., 2018. Meteorological and Hydrological Drought on the Loess Plateau, China: Evolutionary Characteristics, Impact, and Propagation. J. Geophys. Res. Atmos. 123, 11,569-11,584. https://doi.org/10.1029/2018JD029145

Yevjevich, V.M., 1967. Objective approach to definitions and investigations of continental hydrologic droughts, An. Hydrol. Papers (Colorado State University). No. 23.

Yong, B., Ren, L., Hong, Y., Gourley, J.J., Chen, X., Dong, J., Wang, W., Shen, Y., Hardy, J., 2013. Spatial-temporal changes of water resources in a typical semiarid basin of north china over the past 50 years and assessment of possible natural and socio-economic causes. J. Hydrometeorol. 14, 1009–1034. https://doi.org/10.1175/JHM-D-12-0116.1

Yue, W., Gao, J., Yang, X., 2014. Estimation of gross domestic product using multi-sensor remote sensing data: A case study in zhejiang province, east China. Remote Sens. 6, 7260–7275. https://doi.org/10.3390/rs6087260

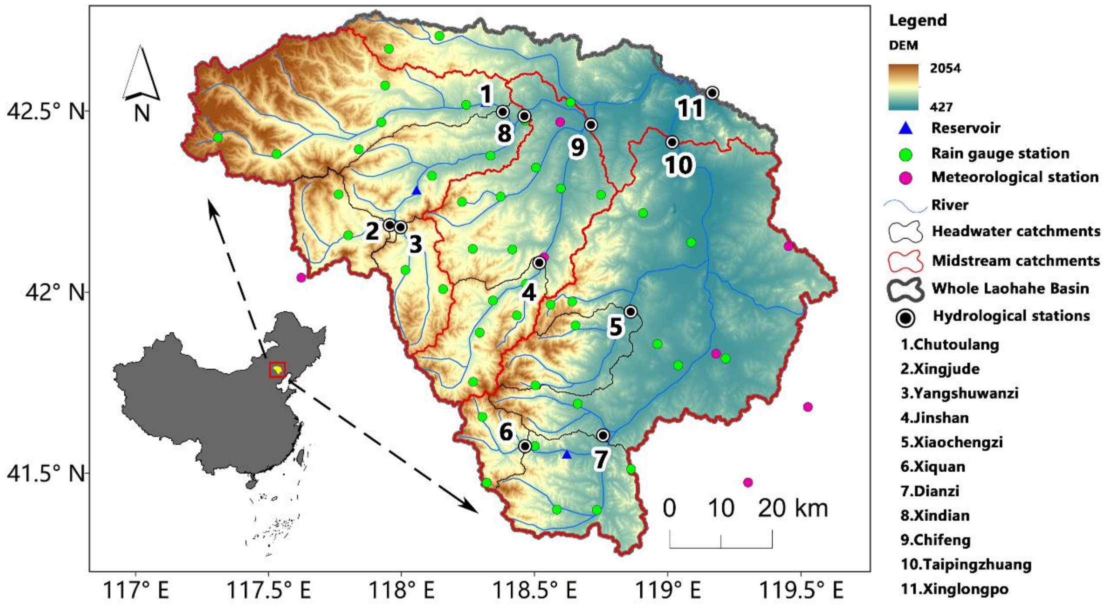

Fig. 1. Location of the Laohahe basin and distribution of hydrological, meteorological, and rain gauge stations.

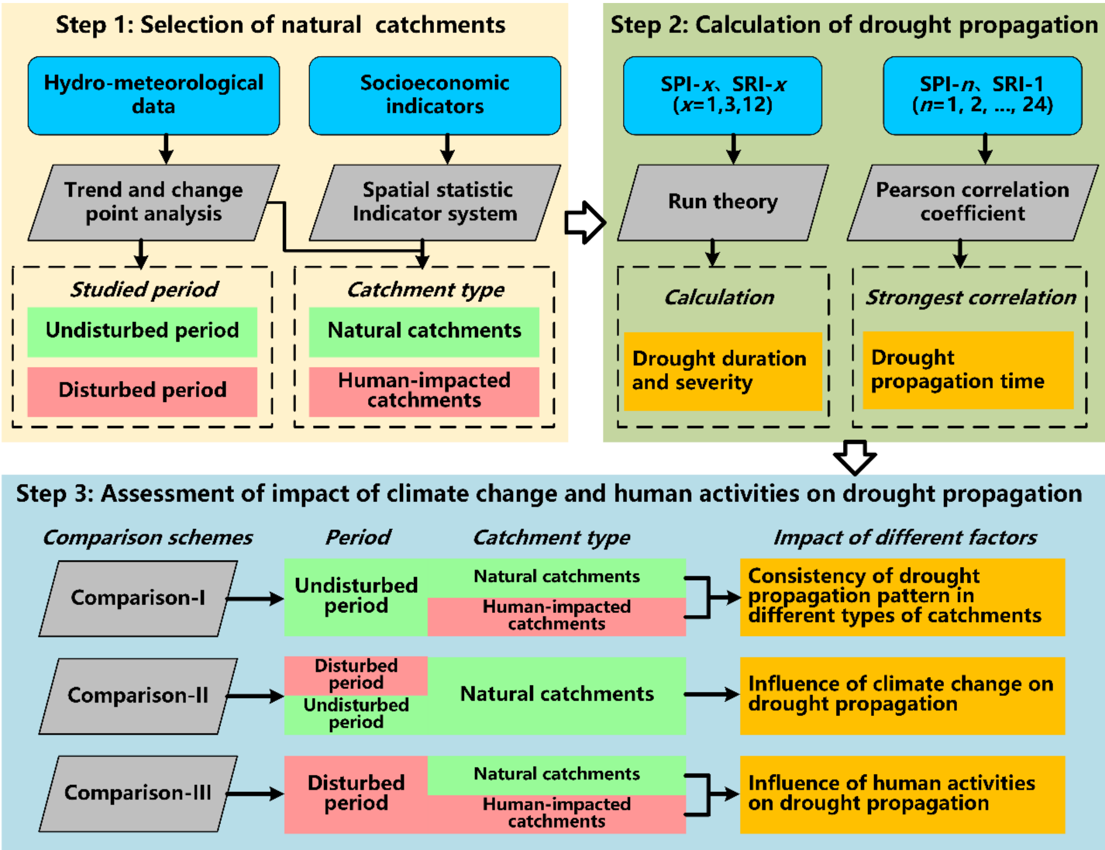

Fig. 2. An observation-based natural and human-impacted catchment comparison method for separating the effects of climate change and human activities on drought propagation.

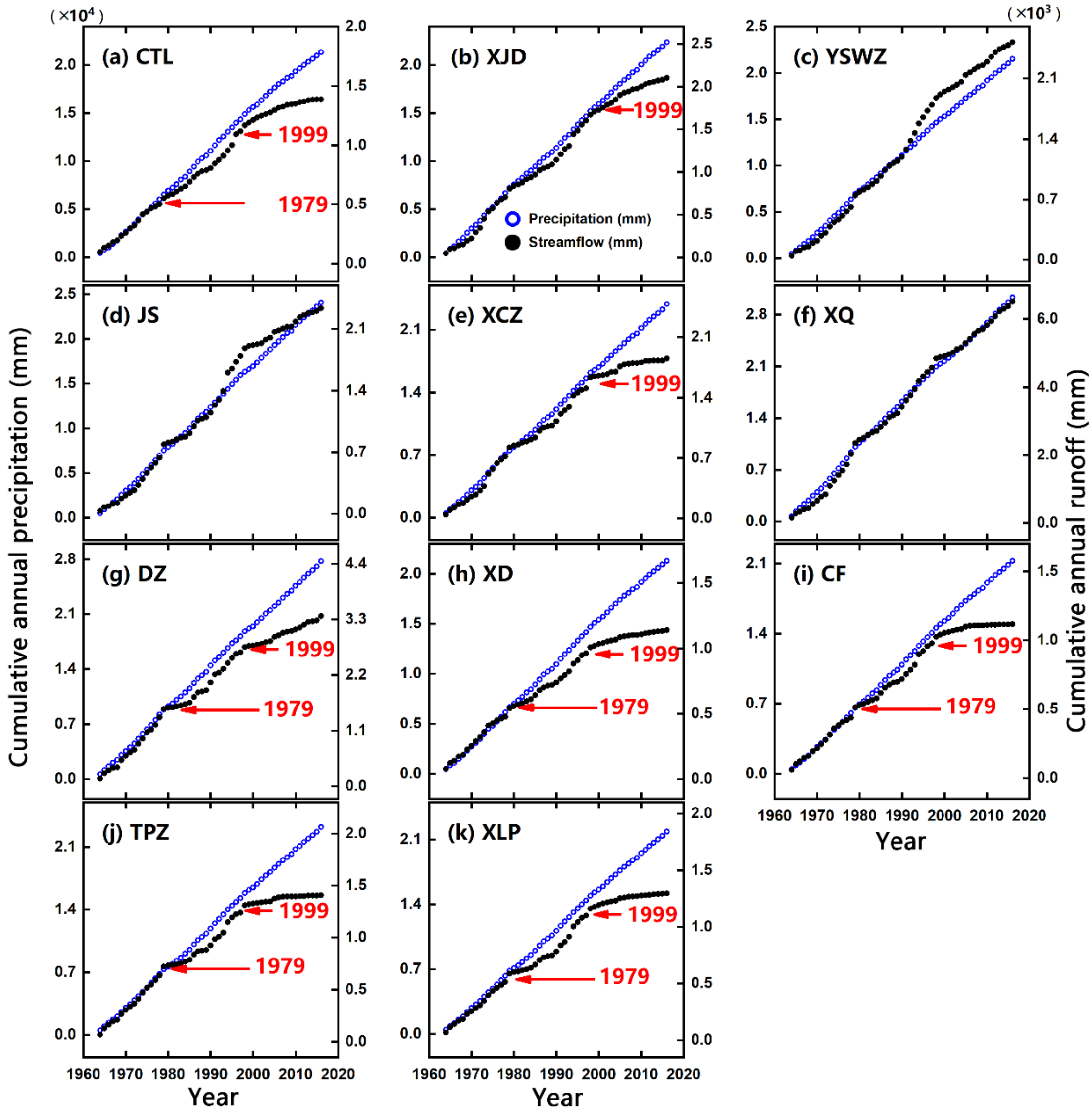

Fig. 3. Double cumulative curves of precipitation and runoff for the 11 selected catchments in the Laohahe basin.

1133 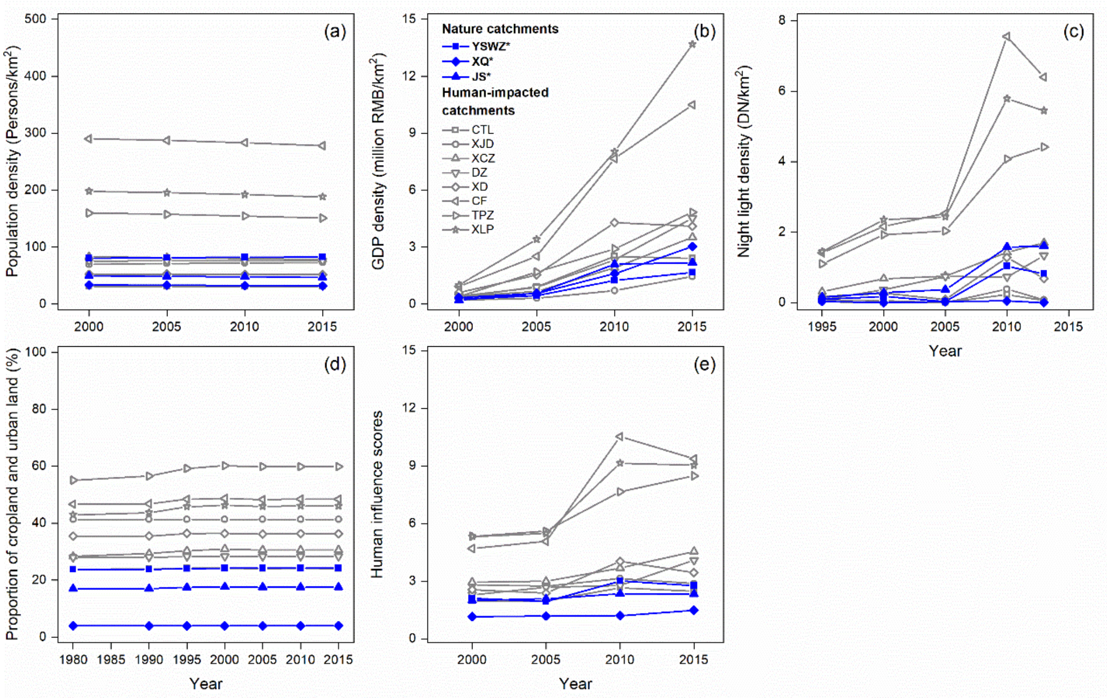

1134 **Fig. 4.** Temporal changes of socio-economic indicators (average population (a), GDP

1135 (b), and night light (c) density), proportion of cropland and urban land (d), and human

1136 influence scores (e) for each catchment in the Laohahe basin.

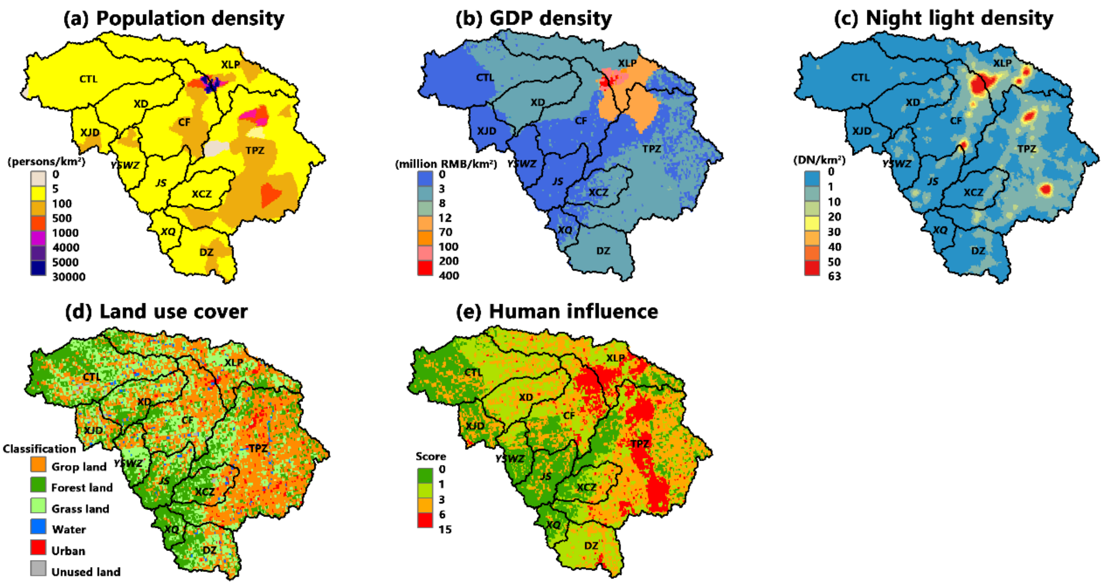

Fig. 5. Spatial distribution of socio-economic indicators, land use data and human influence scores in the Laohahe basin.

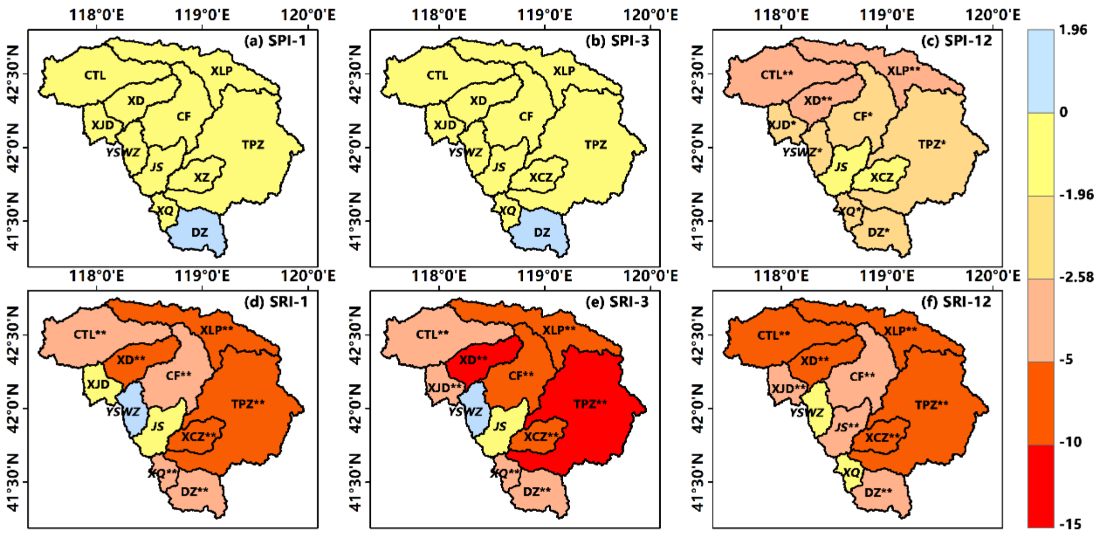

Fig. 6. Modified Mann–Kendall (MMK) trends in the long-term Standardized Precipitation Index and Standardized Runoff Index time series measured at 1-, 3-, and 12-month time scales in 11 catchments of the Laohahe basin from 1964 to 2016. The colour bar denotes the value of the *Z* statistic. "*" and "**" means significance at 0.05 and 0.01 level.

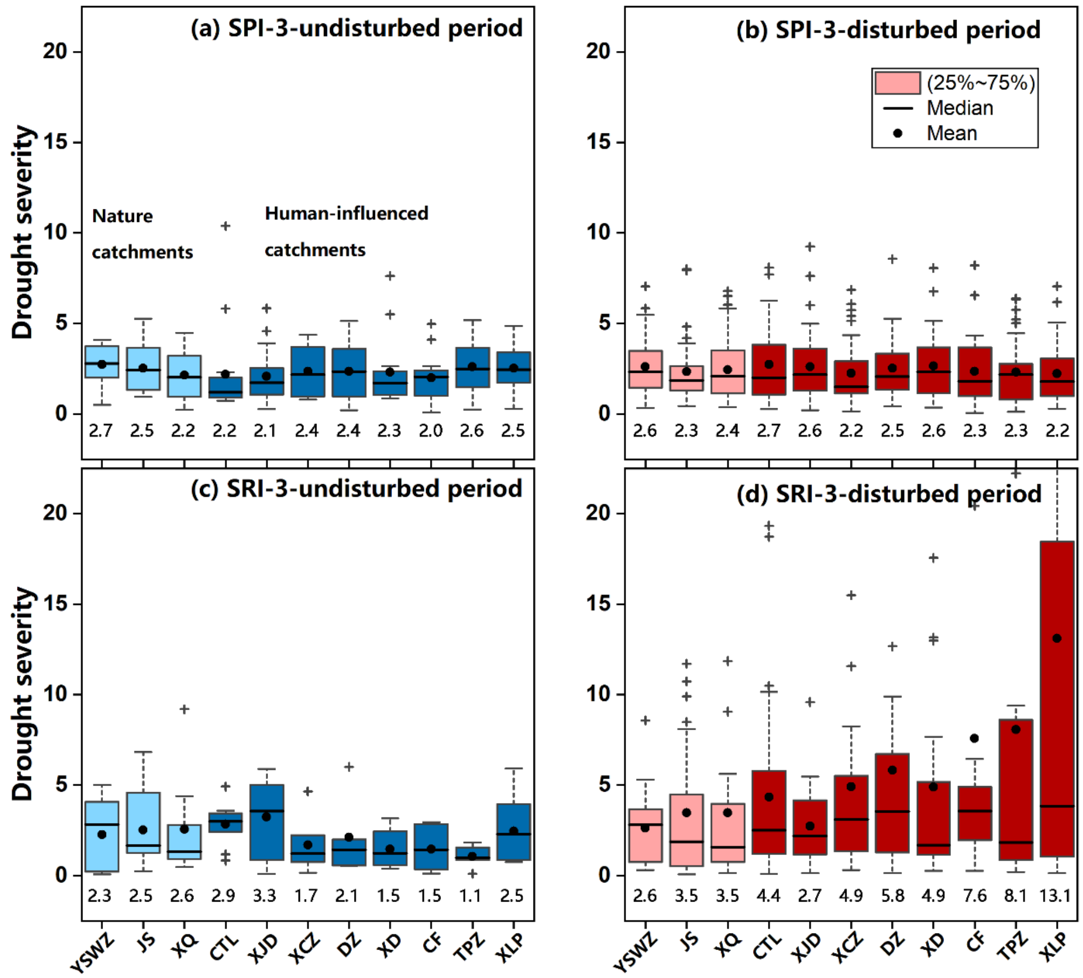

Fig. 7. Box plots of drought severity for meteorological and hydrological drought of 11 catchments in the Laohahe basin during undisturbed and disturbed periods, based on the Standardized Precipitation Index (SPI) and Standardized Runoff Index (SRI) time series measured at 3-month time scales. The numbers within the figure are the average severity of meteorological and hydrological drought.

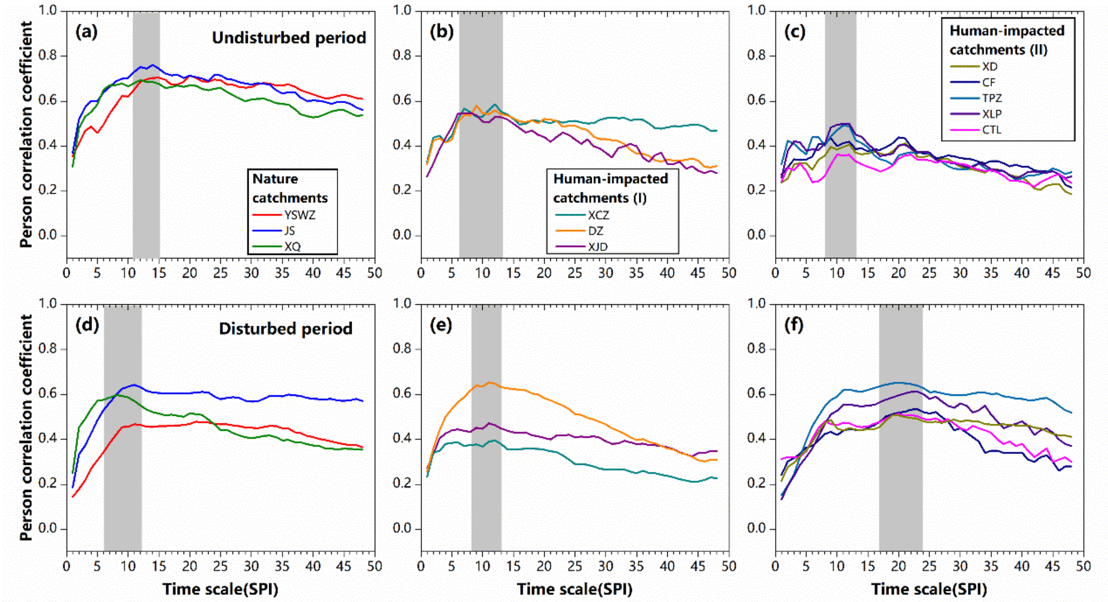

Fig. 8. PCCs for the cross-correlation between the SRI-1 series and the SPI series at various time scales for all 11 catchments ((a) and (d) for natural catchments; (b), (c), (e), and (f), for human-influenced catchments) during undisturbed (top) and disturbed (bottom) periods. The grey shading indicates the range of time scales with the maximum PCC.

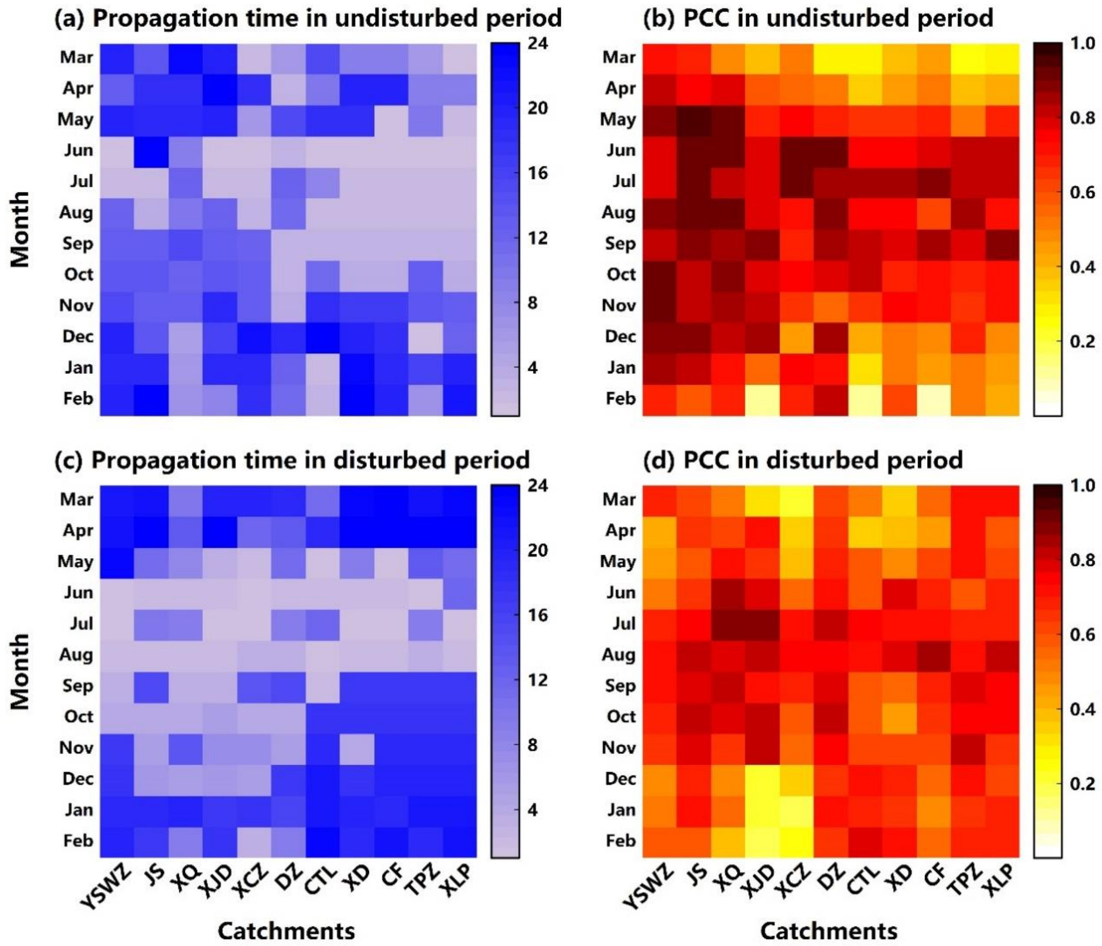

Fig. 9. Seasonal variability in the drought propagation time during (a) undisturbed and (c) disturbed periods and the corresponding maximum PCC for each month in each catchment ((b) and (d)). The colour bars indicate the drought propagation time in months (left) and the maximum PCC (right).

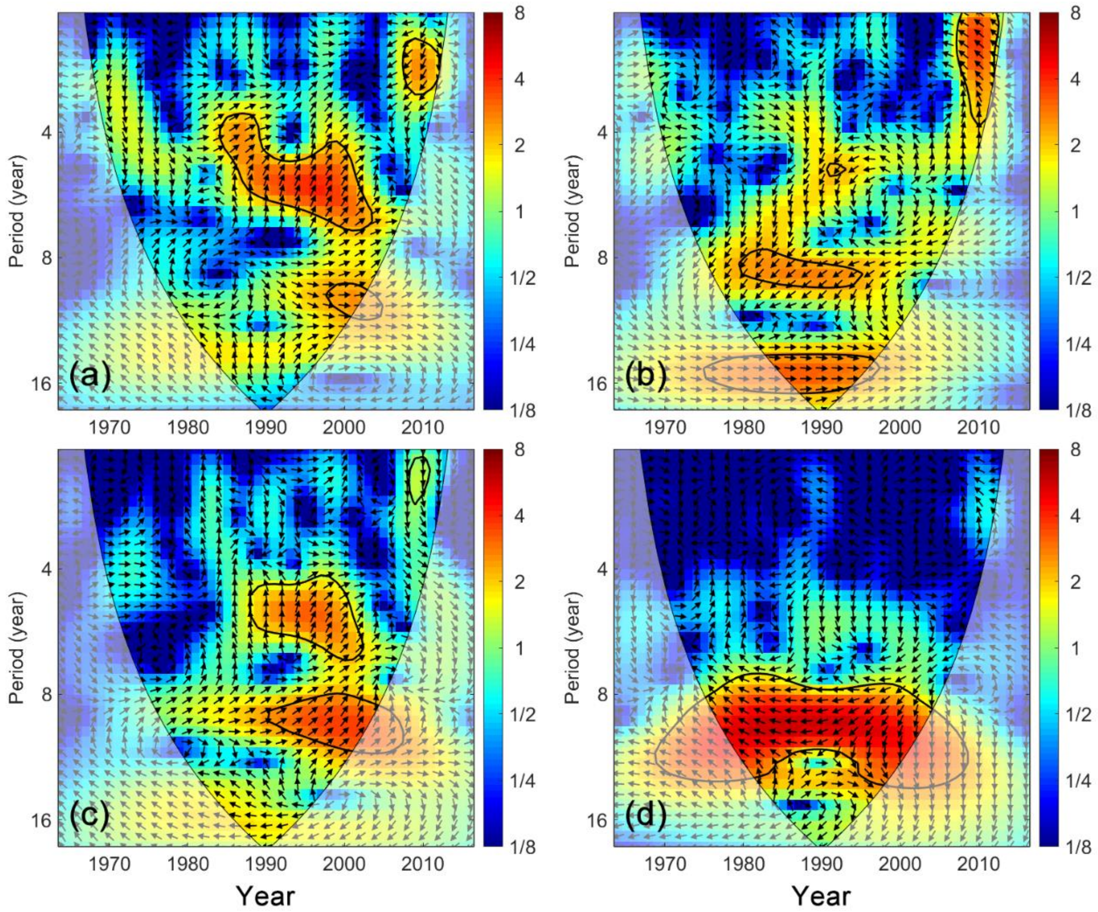

Fig. 10. The cross wavelet transforms between annual actual evaporation in the JS catchment and average monthly (a) ENSO, (b) AO, (c) PDO and (d) sunspot values during 1964–2016. The 95% confidence level against the red noise is exhibited as a thick contour, and the relative phase relationship is denoted as arrows (with negative correlations pointing left and positive associations pointing right). The colour bar on the right denotes the wavelet energy.

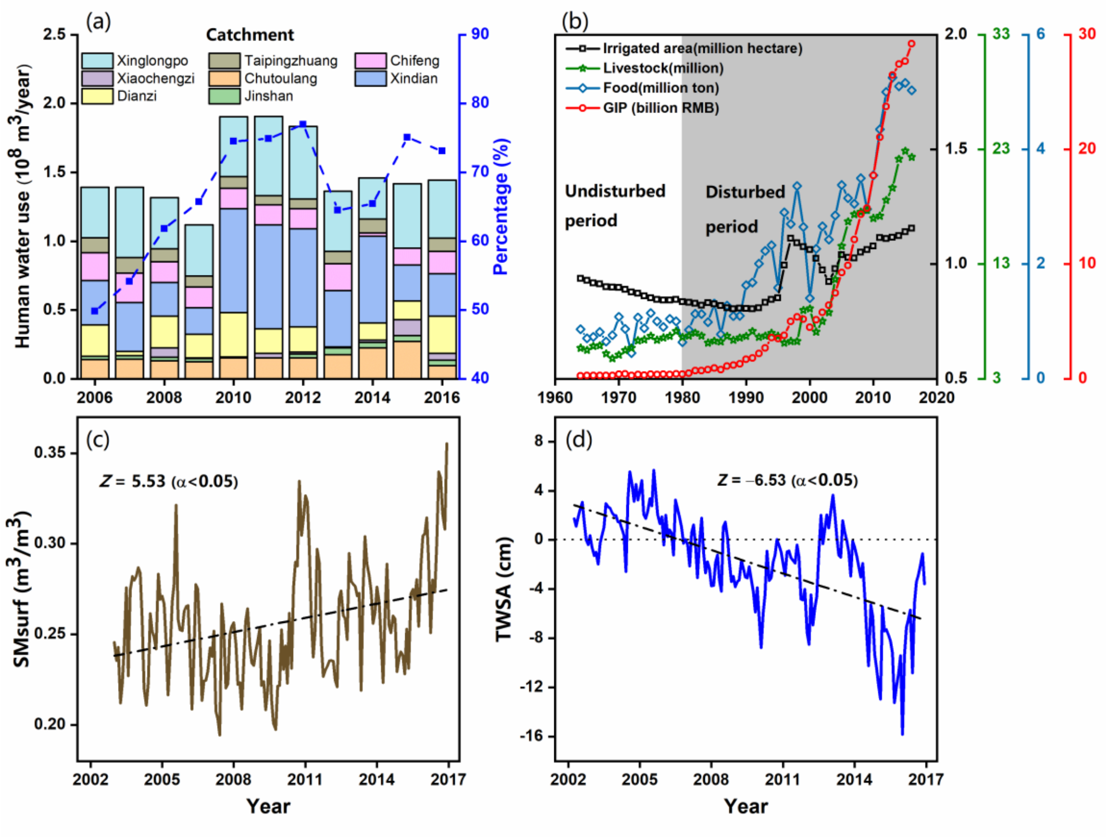

Fig. 11. (a) Annual water withdrawal for each catchment and the percentage of total withdrawal to natural runoff for the Laohahe basin during 2006–2016, (b) changes in agricultural and industrial production data for the study area during 1964–2016 (undisturbed period and disturbed period), and time series of (c) surface soil moisture (SMsurf) and (d) terrestrial water storage anomalies (TWSA) during 2003–2016 (the Z value is calculated by the MMK test method).

Table 1

Characteristics of the selected catchments in the Laohahe basin.

Catchment	Hydrological station	Abbreviation	Area (km^2)	Lon (E°)	Lat (N°)	Mean annual precipitation (mm/year)	Mean annual runoff (mm/year)	Data period
1	Chutoulang	CTL	2869	118.62	42.35	402.61	26.17	1964-2016
2	Xingjude	XJD	697	118.13	42.08	422.70	39.65	1964-2016
3	Yangshuwanzi	YSWZ	674	118.17	42.07	398.97	49.46	1964-2016
4	Jinshan	JS	1034	118.68	41.92	453.60	44.03	1964-2016
5	Xiaochengzi	XCZ	866	119.00	41.75	450.57	34.89	1964-2016
6	Xiquan	XQ	419	118.53	41.42	572.88	122.80	1964-2016
7	Dianzi	DZ	1643	118.83	41.42	523.26	63.42	1964-2016
8	Xindian	XD	5580	118.70	42.33	401.50	21.50	1964-2016
9	Chifeng	CF	8678	118.95	42.28	401.00	21.06	1964-2016
10	Taipingzhuang	TPZ	7720	119.25	42.20	438.53	26.57	1964-2016
11	Xinglongpo	XLP	18112	119.43	42.32	411.74	24.48	1964-2016

Notes: The Xinglongpo streamflow station of was built in 1976, and the streamflow data before 1976 are substituted by those recorded at the adjacent Xiaoheyan station (42.32°N, 119.43°E).

Table 2

Detail information of remote sensing inversion and reanalysis data used in this study.

Data types	Temporal and spatial coverage	Units	Data sources
DEM	2012/30″	m	U.S. Geological Survey (USGS) website (https://www.usgs.gov/).
ENSO, PDO, AO	1964-2016/—	—	NOAA Physical Sciences Laboratory (PSL) (https://psl.noaa.gov/data/climateindices/);
Sunspot data	1964-2016/—	—	Royal Observatory of Belgium (http://www.sidc.be/sunspot-data)
Surface soil moisture	2003-2016/0.1°	m^3/m^3	(Chen et al., 2021) (https://doi.org/10.1594/PANGAEA.912597).
Gravity recovery and climate experiment (GRACE) data	2003-2016/0.25°	cm	GRACE RL06 CSR mascon solutions (http://www2.csr.utexas.edu/grace); (Wei et al, 2021)
Land use and cover	1980, 1990, 1995, 2000, 2005, 2010, 2015/~1 km	—	Data Centre for Resources and Environmental Sciences, Chinese Academy of Sciences (RESDC) (http://www.resdc.cn)
GDP density	2000, 2005, 2010, 2015/~1 km	million RMB/km^2	Same as Land use and cover
Population density	2000, 2005, 2010, 2015/~1 km	persons/ km^2	NASA Socio-economic Data and Applications Center (SEDAC). (https://doi.org/10.7927/H49C6VHW)
Night light density	1995, 2000, 2005, 2010, 2013/~1 km	DN/km^2	NOAA's National Geophysical Data Center (https://www.ngdc.noaa.gov/eog/dmsp/download V4composites.html)

Notes: The DN value represents the average light intensity in the range of 0–63, and the larger the DN value, the higher the light intensity

Table 3

Classification and the corresponding scores of indictors reflecting human influence.

Data set	Grade	Score	Reference
Population density	0-278	1	(Perkl, 2016)
(persons/km^2)	278-390	2	
	390-501	3	
	501-612	4	
	>612	5	
GDP density	0-3	1	(Han et al., 2012)
(million RMB/km^2)	3-20	2	
	20-50	3	
	50-100	4	
	>100	5	
Night light density	0-12	0	(Small et al., 2011; Ma et al., 2012)
(DN/km^2)	>12	1	
Land cover	Cropland	3	(Theobald et al. 2010; Perkl, 2016)
	Urban land	4	
	others	0	

Note: The DN value represents the average light intensity in the range of 0–63, and the larger the DN value, the stronger the light intensity.

Table 4

Results of the trend analysis and change point tests of annual precipitation (P), PET, and runoff (R) for the selected catchments during the period of 1964–2016.

Catchments	MMK trend test (year)			Pettitt test for the change point (year)			Heuristic segmentation test for the change point (year)		
	P	PET	R	P	PET	R	P	PET	R
CTL	–1.57 ↓	–1.47 ↓	–4.46 ↓ **	—	—	1979*,1999**	—	—	1999**
XJD	–1.10 ↓	–0.97 ↓	–2.82 ↓ **	—	—	1999**	—	—	1998*
YSWZ	–0.66 ↓	–0.93 ↓	–0.40 ↓	—	—	—	—	—	—
JS	–0.65 ↓	–0.25 ↓	–0.88 ↓	—	—	—	—	—	—
XCZ	–1.00 ↓	–0.18 ↓	–4.18 ↓ **	—	—	1998**	—	—	1999**
XQ	–1.36 ↓	–1.20 ↓	–0.48 ↓	—	—	—	—	—	—
DZ	–0.51 ↓	–0.21 ↓	–1.71 ↓ *	—	—	1979**,1999*	—	—	1979*,1999*
XD	–1.33 ↓	–1.11 ↓	–3.94 ↓ **	—	—	1979**,1999**	—	—	1979**,1999**
CF	–0.72 ↓	–0.64 ↓	–4.12 ↓ **	—	—	1979*,1999**	—	—	1979*,1999**
TPZ	–0.60 ↓	0.31 ↑	–4.10 ↓ **	—	—	1979**,1999**	—	—	1979**,1999**
XJD	–0.94 ↓	–0.70 ↓	–5.04 ↓ **	—	—	1979**,1999**	—	—	1979*,1999**

Notes: ‘ ↓ ’ and ‘ ↑ ’ indicate downward and upward trends, respectively. ‘*’ and ‘**’ denote significance at the 95% and 99% confidence levels, respectively.

Table 5

Summary of average human influence scores during 2000-2015 and reservoirs information for the 11 selected catchments (human-impacted catchments are divided into two groups according to catchment area, as shown in Fig. 8).

Group	Natural catchments (catchment area < 2000 km^2)			Human-impacted catchments (I) (catchment area < 2000 km^2)			Human-impacted catchments (II) (catchment area > 2000 km^2)				
Catchment	YSWZ	JS	XQ	XCZ	DZ	XJD	CTL	XD	CF	TPZ	XLP
HI scores	2.46	2.19	1.26	3.54	3.16	3.19	3.27	3.11	7.42	6.77	7.24
Reservoir	No	No	No	No	Yes	No	Yes	Yes	Yes	Yes	Yes

Table 6

Differences in average drought characteristics calculated from SPI-3 and SRI-3 series between undisturbed and disturbed periods for the selected 11 catchments in the Laohahe basin.

Types	Catchments	Average drought duration (%)		Average drought severity (%)	
		SPI-3	SRI-3	SPI-3	SRI-3
Natural catchments	YSWZ	–3.8	41.2	–5.1	3.2
	JS	–0.6	70.7	–6.8	93.1
	XQ	6.9	30.3	13.5	35.0
	Mean	0.8	47.4	0.5	43.8
Human-impacted catchments (I)	XCZ	–3.2	224.1	–5.1	189.4
	DZ	–3.1	125.8	6.8	175.8
	XJD	12.7	–6.1	24.9	–32.2
	Mean	2.1	114.6	8.9	110.7
Human-impacted catchments (II)	CTL	11.5	26.3	25.2	52.6
	XD	1.7	123.6	18.9	232.7
	CF	8.5	263.8	18.2	418.5
	TPZ	–2.1	176.3	–10.8	653.3
	XLP	–6.6	376.2	–12.3	1236.7
	Mean	2.6	193.2	7.8	518.8

Table 7

Differences in the drought propagation time for different comparison schemes.

Comparison schemes	Period	Catchments types	Drought propagation time (months)		
			Mean	Median	Max.
I	Undisturbed	Natural	12.7	12.0	14.0
	——	Human-impacted (I)	9.0	9.0	12.0
	Difference	(months)	–3.0	–3.0	–2.0
	——	Human-impacted (II)	10.4	11.0	12.0
	Difference	(months)	–2.0	–1.0	–2.0
Ⅱ	Undisturbed	Natural	12.7	12.0	14.0
	Disturbed	Natural	9.3	9.0	11.0
	Difference	(months)	–3.0	–3.0	–3.0
Ⅲ	Disturbed	Natural	9.3	9.0	11.0
	——	Human-impacted (I)	11.3	11.0	12.0
	Difference	(months)	+2.0	+2.0	+1.0
	——	Human-impacted (II)	21.0	20.0	23.0
	Difference	(months)	+12.0	+11.0	+12.0

Note: Propagation time indicates the SPI accumulation period (SPI-n) most strongly correlated with SRI-1. A negative change (–) means that the SPI accumulation period becomes shorter; a positive change (+) means that the SPI accumulation period becomes longer.

Credit Author Statement

Menghao Wang: Conceptualization, Methodology, Software.

Shanhu Jiang: Conceptualization, Project administration.

Liliang Ren: Funding acquisition.

Chong-Yu Xu and Lucas Menzel: Writing-Review & Editing.

Fei Yuan, Qin Xu, Yi Liu, and Xiaoli Yang: Methodology.

The authors declare that they have no known competing financial interests or personal relationships that could have appeared to influence the work reported in this paper.

Figure1

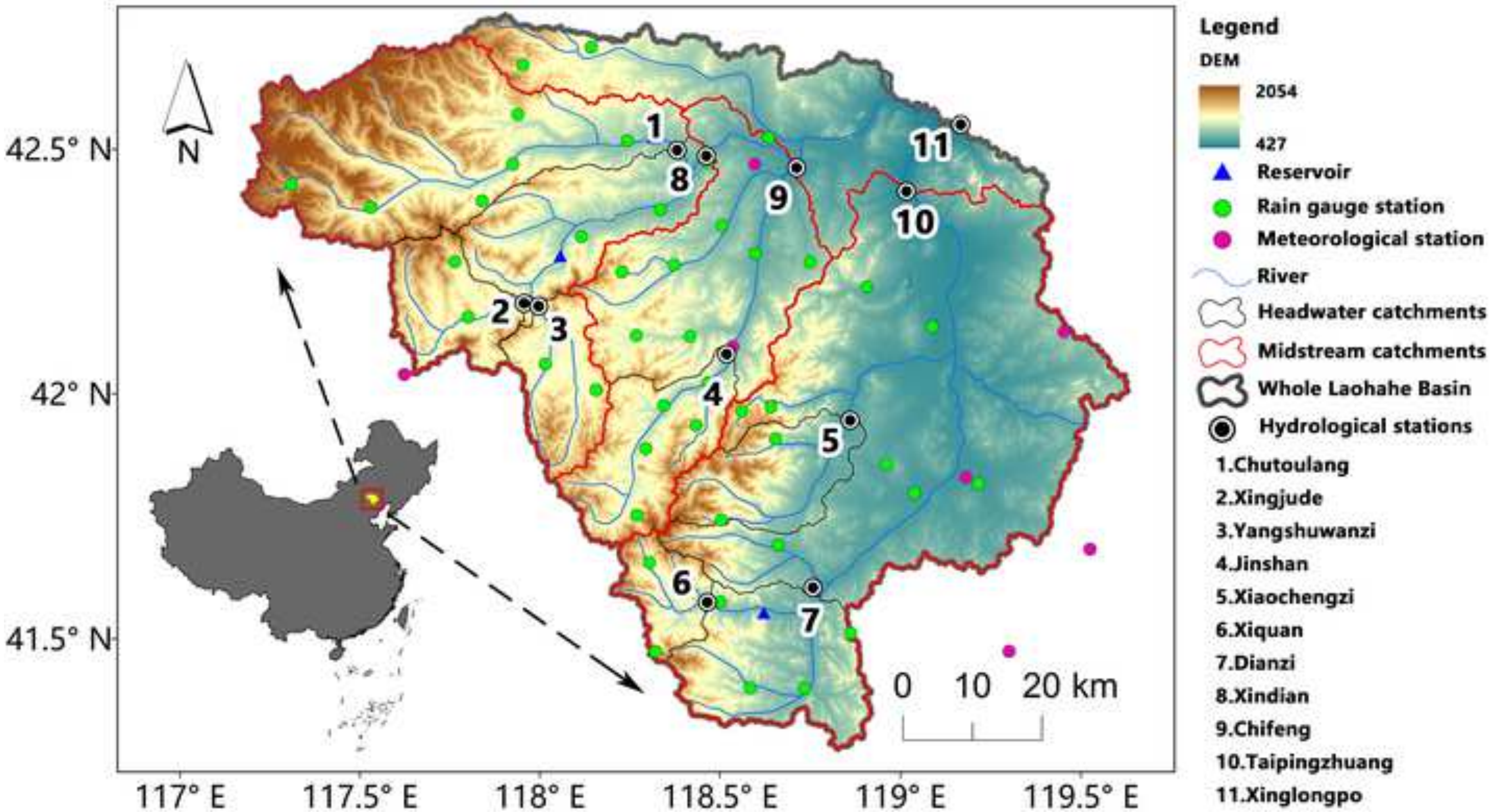

Legend
DEM
2054
427
Reservoir
Rain gauge station
Meteorological station
River
Headwater catchments
Midstream catchments
Whole Laohahe Basin
Hydrological stations
1.Chutoulang
2.Xingjude
3.Yangshuwanzi
4.Jinshan
5.Xiaochengzi
6.Xiquan
7.Dianzi
8.Xindian
9.Chifeng
10.Taipingzhuang
11.Xinglongpo
N
42.5° N
42° N
41.5° N
117° E
117.5° E
118° E
118.5° E
119° E
119.5° E
0 10 20 km

Figure2

Click here to access/download;Figure;FIG-2.tif

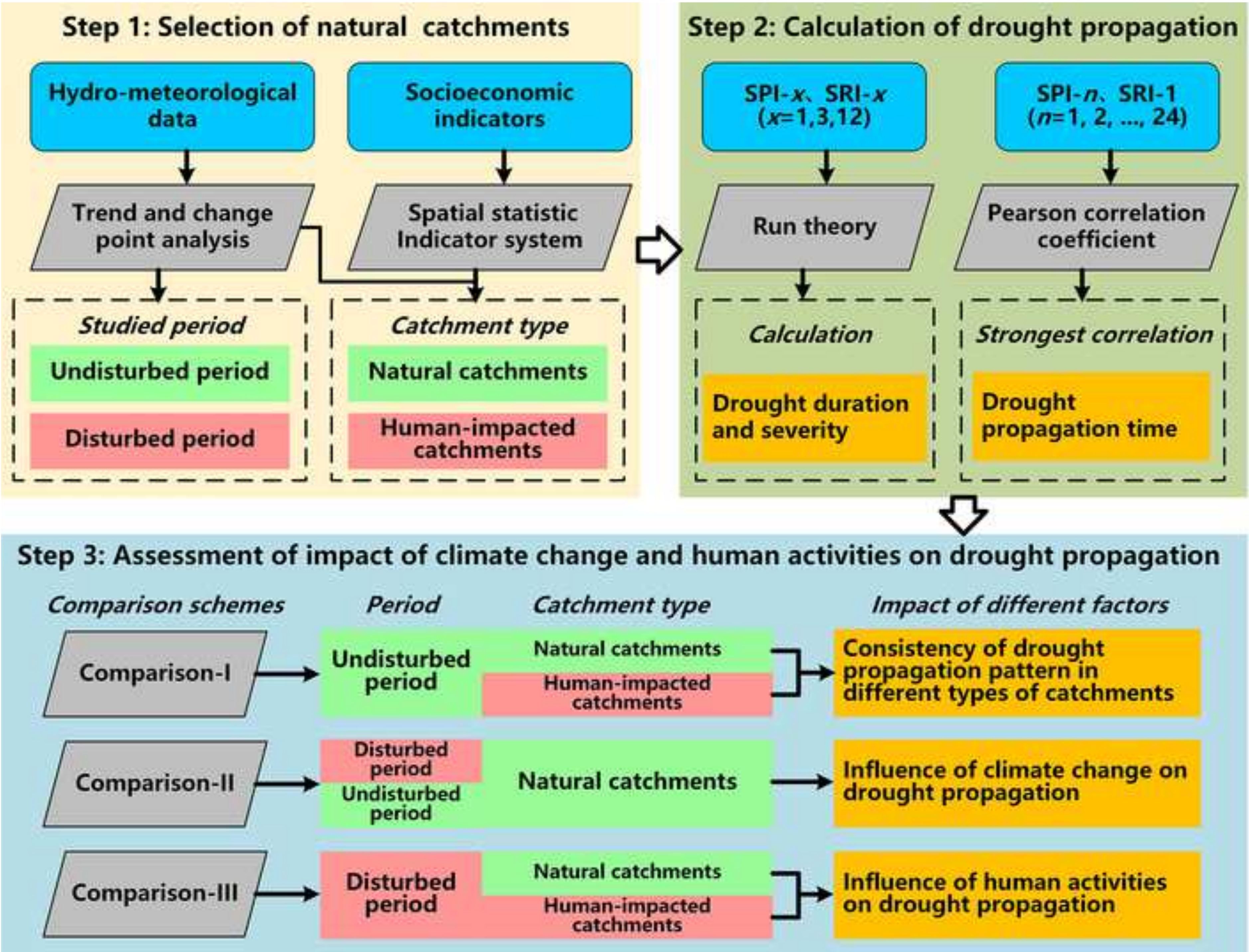

Figure3

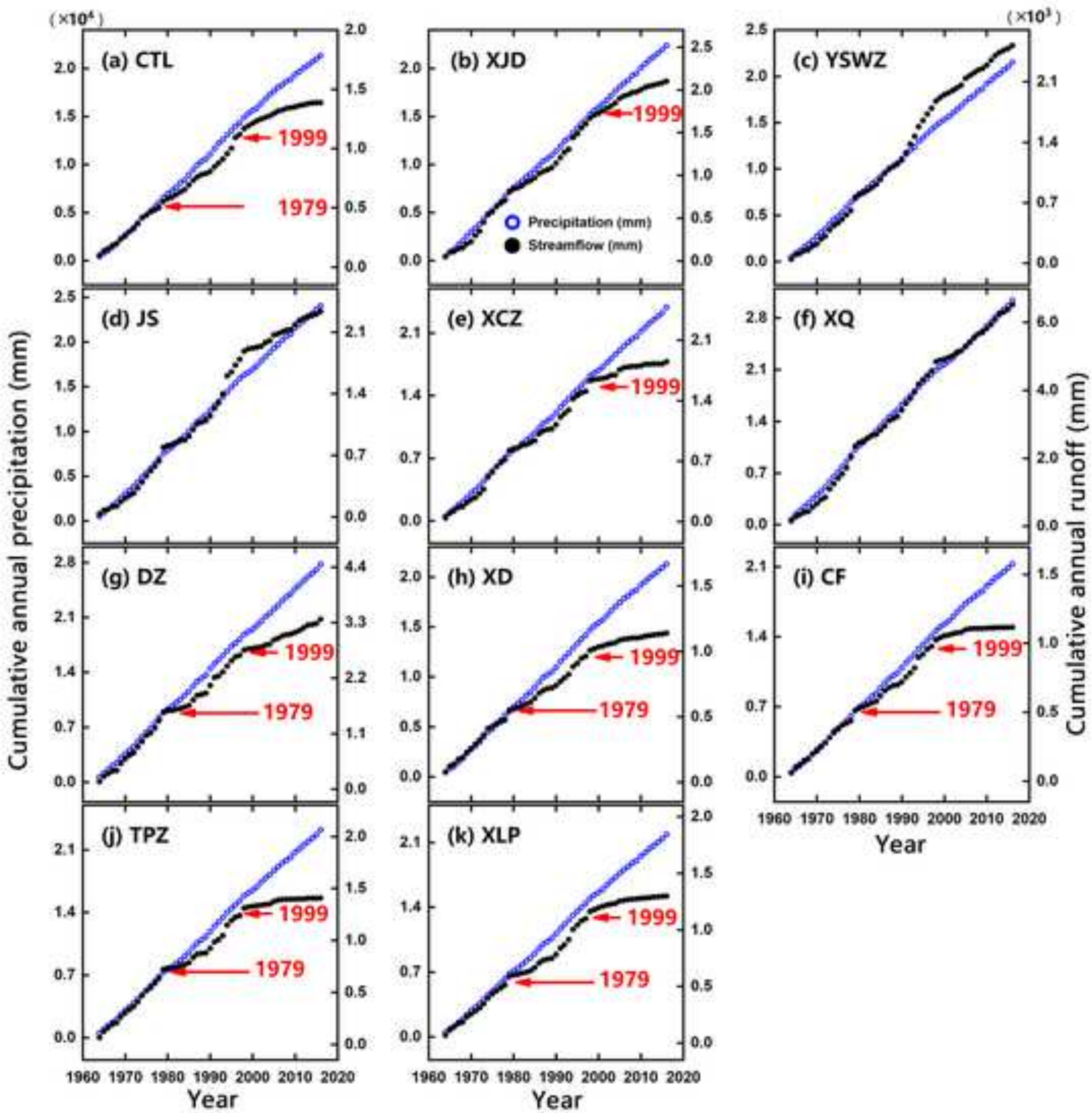

(×10⁴)
(×10³)
(a) CTL
(b) XJD
(c) YSWZ
(d) JS
(e) XCZ
(f) XQ
(g) DZ
(h) XD
(i) CF
(j) TPZ
(k) XLP
1999
1979
Precipitation (mm)
Streamflow (mm)
Cumulative annual precipitation (mm)
Cumulative annual runoff (mm)
Year
1960 1970 1980 1990 2000 2010 2020

Figure4

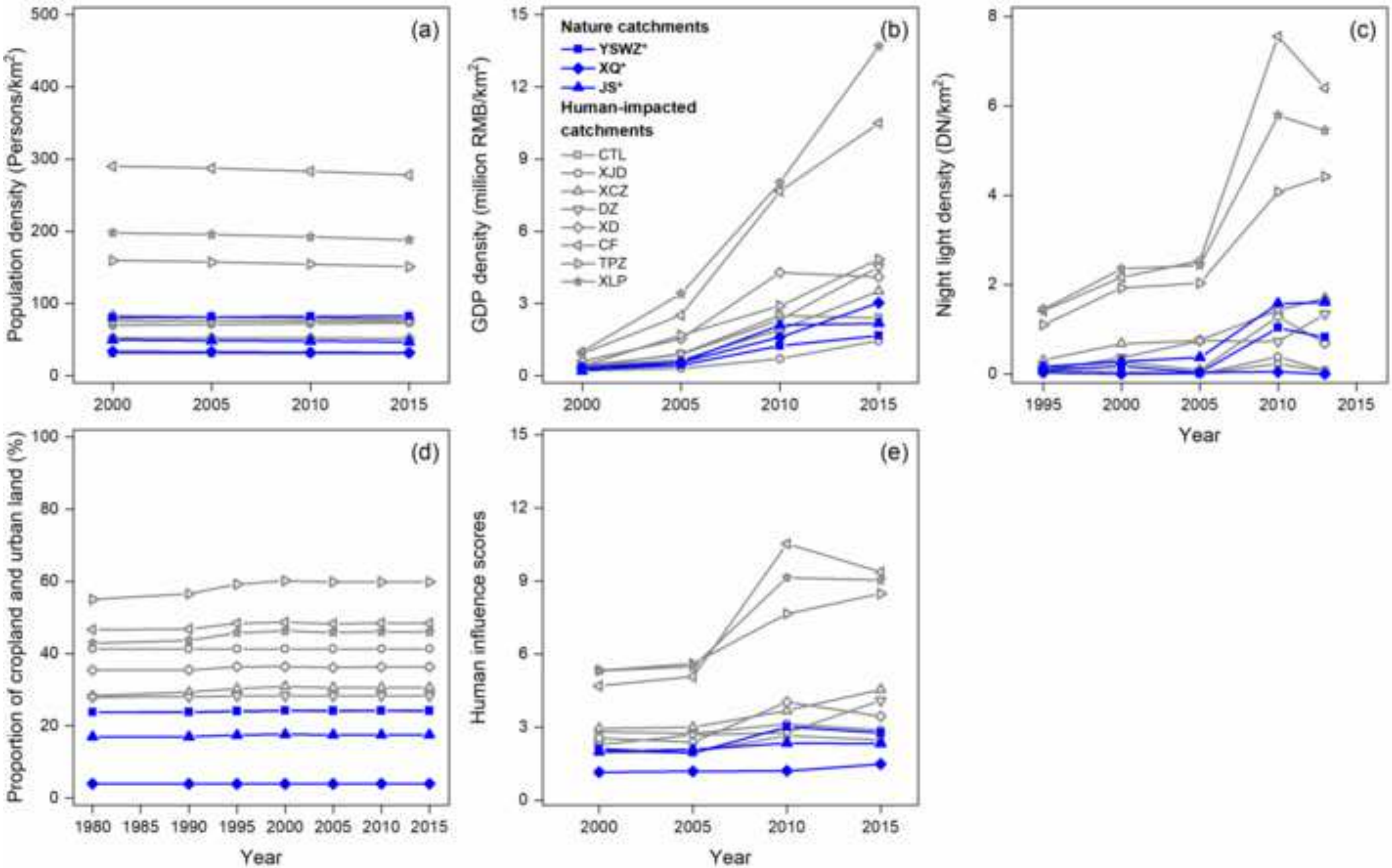
(a)
Population density (Persons/km2)
500
400
300
200
100
0
2000
2005
2010
2015
(b)
GDP density (million RMB/km2)
Nature catchments
YSWZ*
XQ*
JS*
Human-impacted catchments
CTL
XJD
XCZ
DZ
XD
CF
TPZ
XLP
(c)
Night light density (DN/km2)
1995
2000
2005
2010
2015
Year
(d)
Proportion of cropland and urban land (%)
1980
1985
1990
1995
2000
2005
2010
2015
Year
(e)
Human influence scores
2000
2005
2010
2015
Year

Figure5

Click here to access/download;Figure;FIG-5.tif

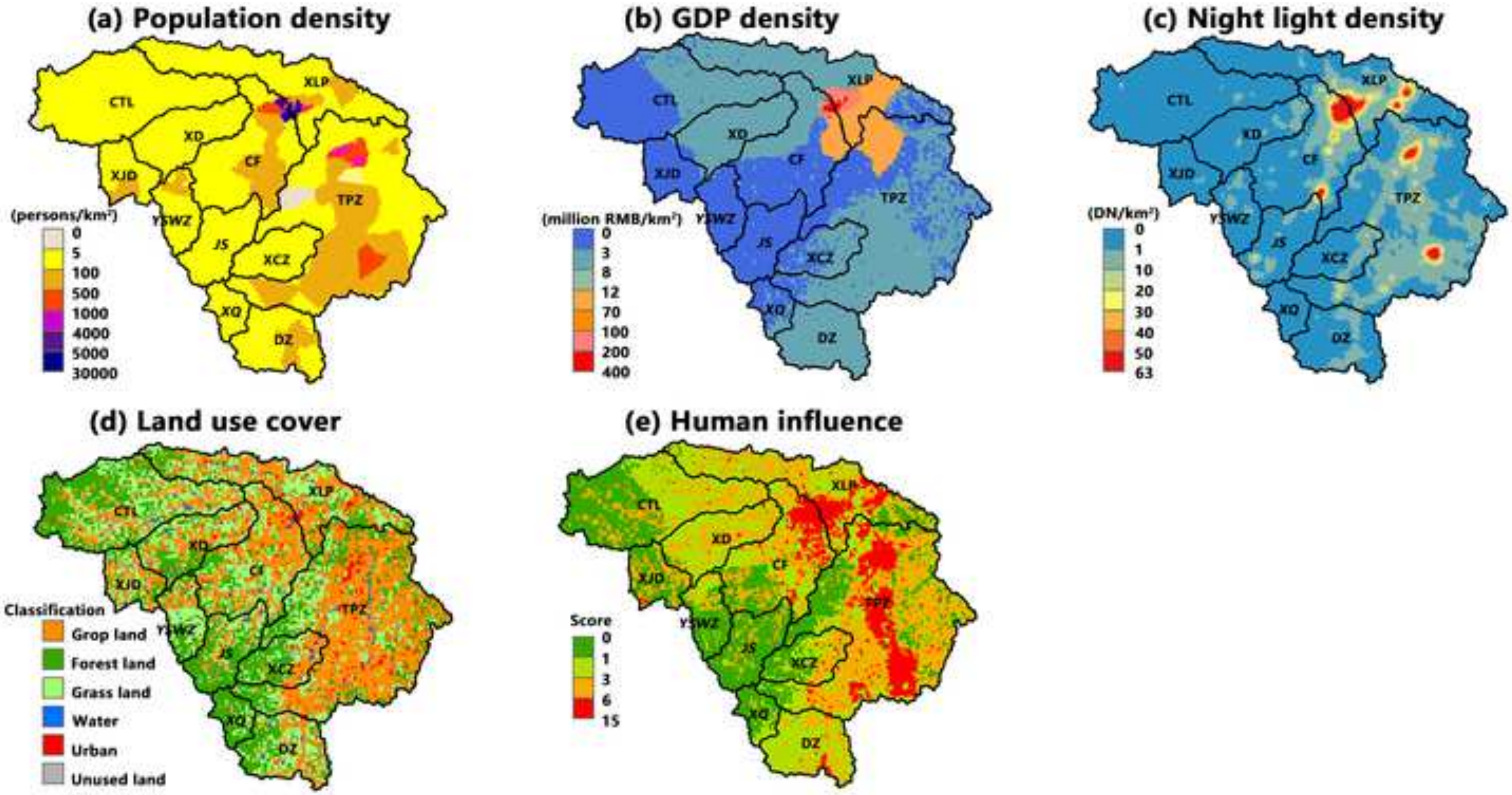

Figure6

Click here to access/download;Figure;FIG-6.tiff

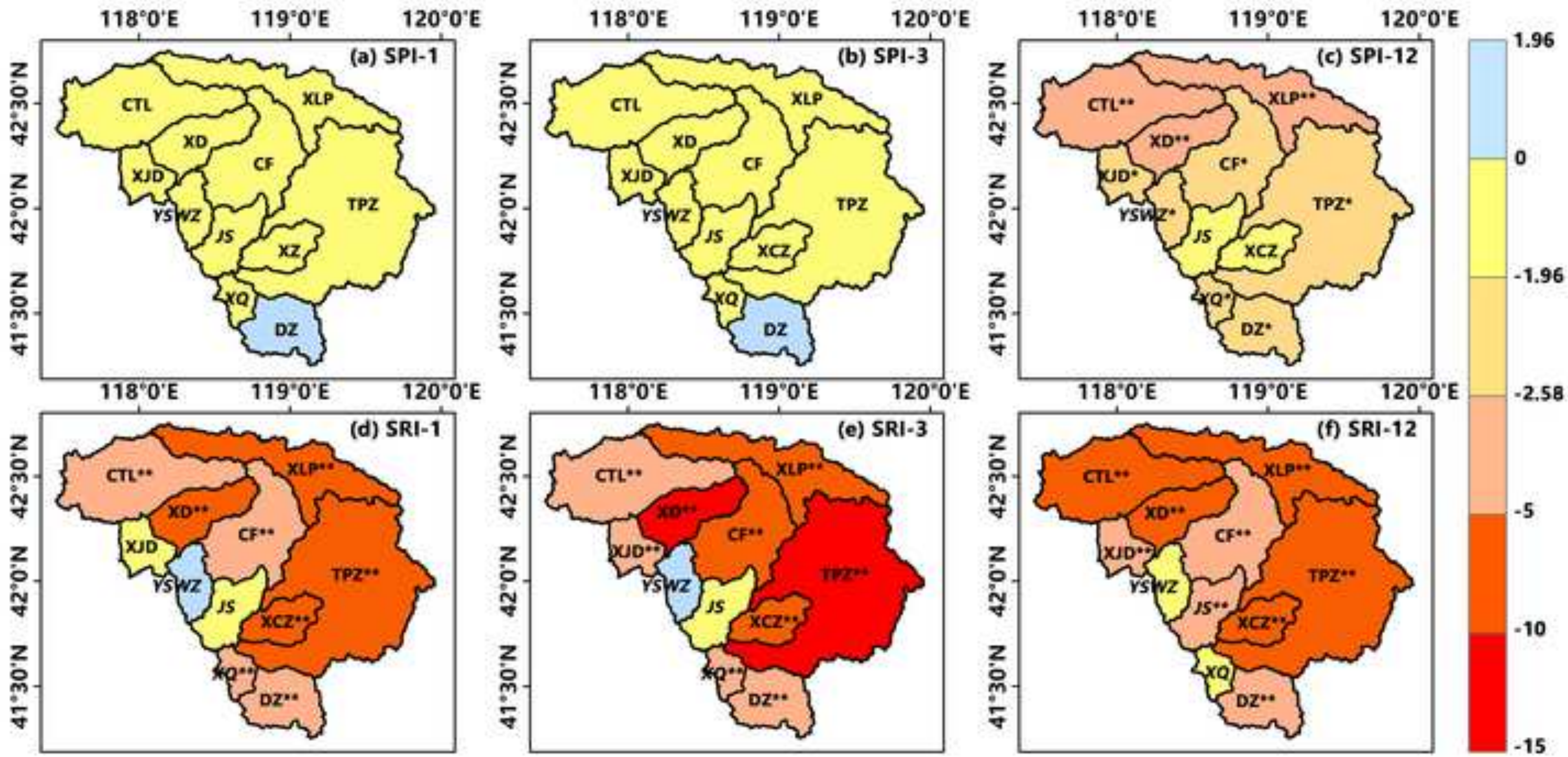

Figure7

Click here to access/download;Figure;FIG-7.tif

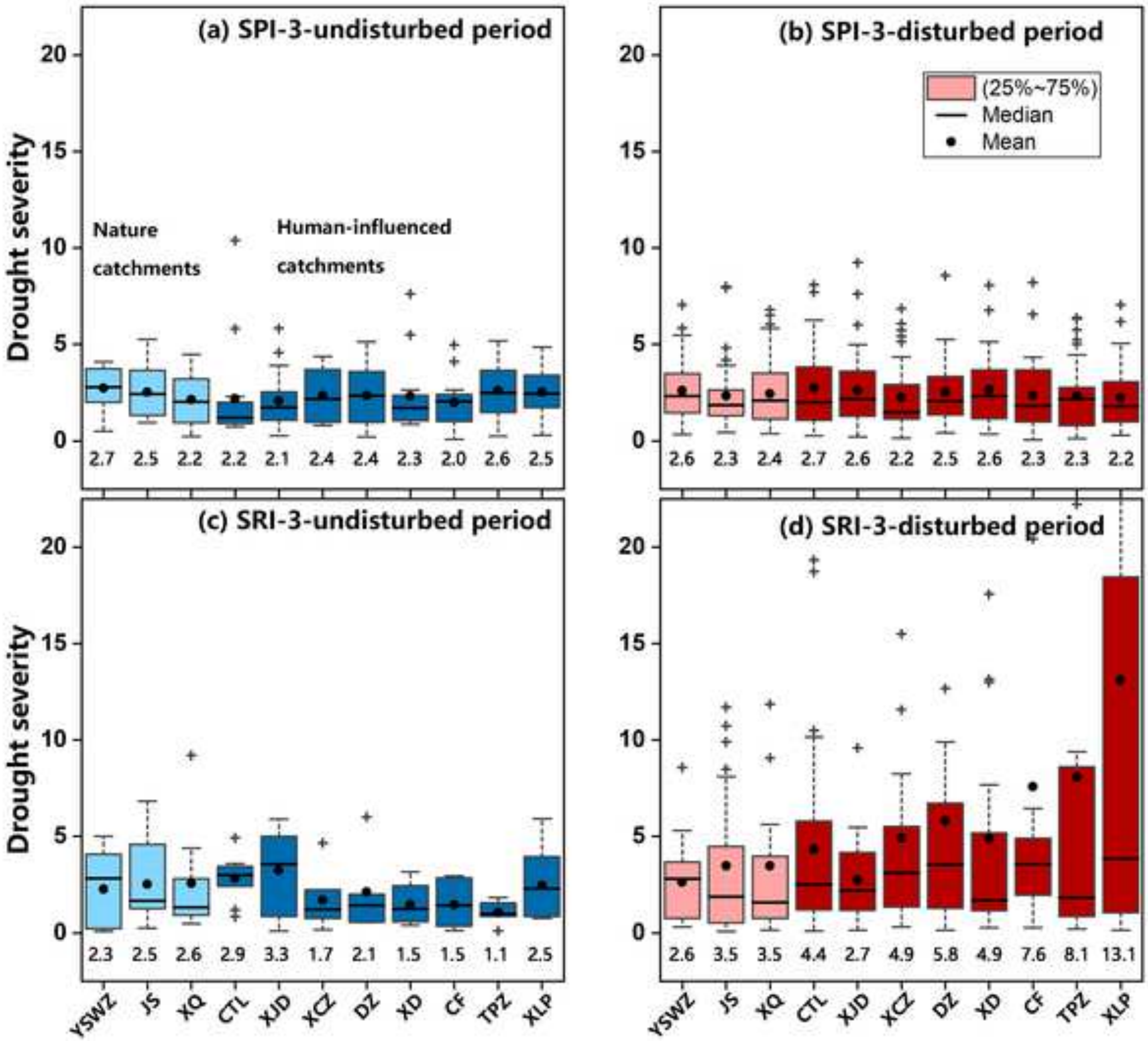

Figure8

Click here to access/download;Figure;FIG-8.tif

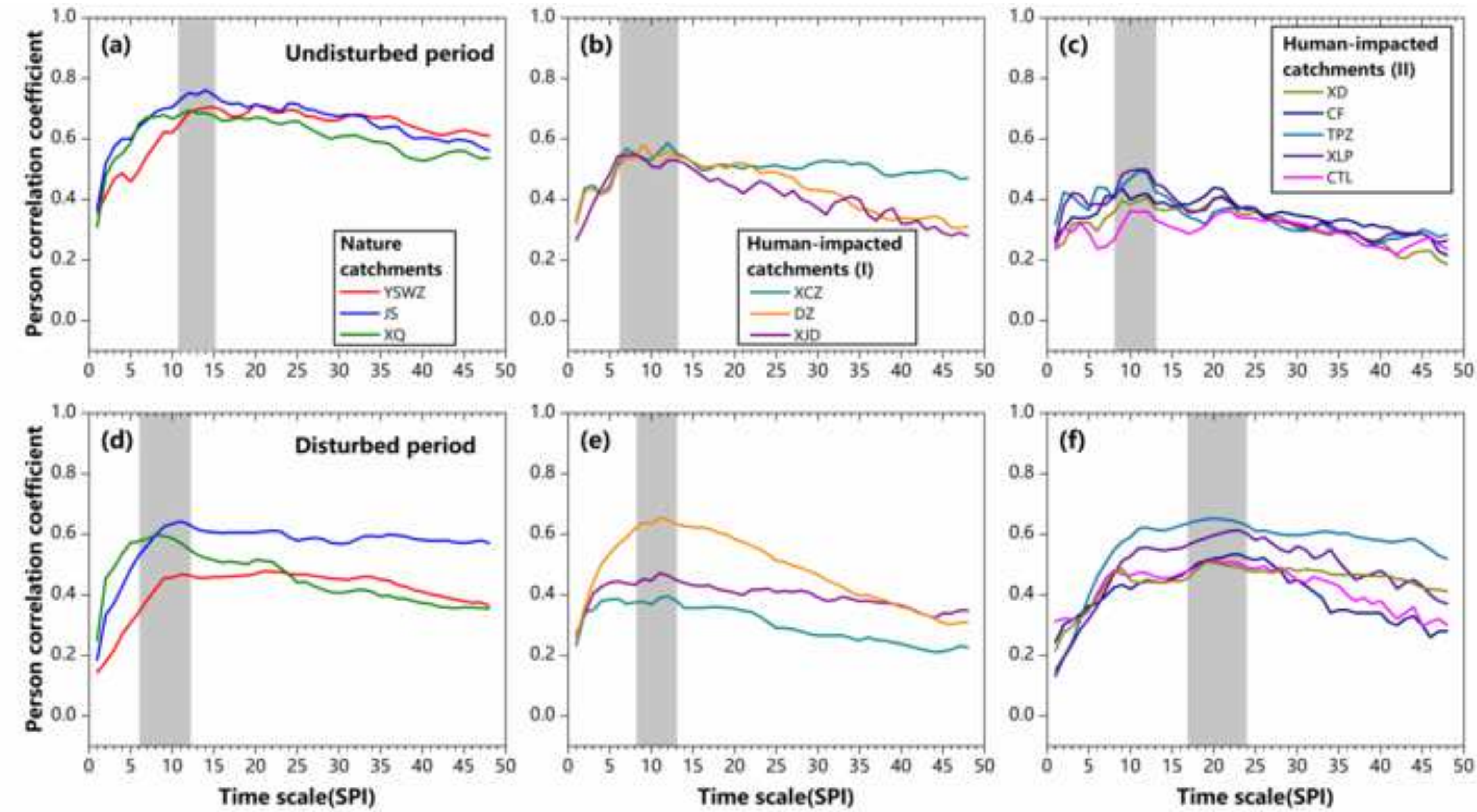

Figure9

Click here to access/download;Figure;FIG-9.tif

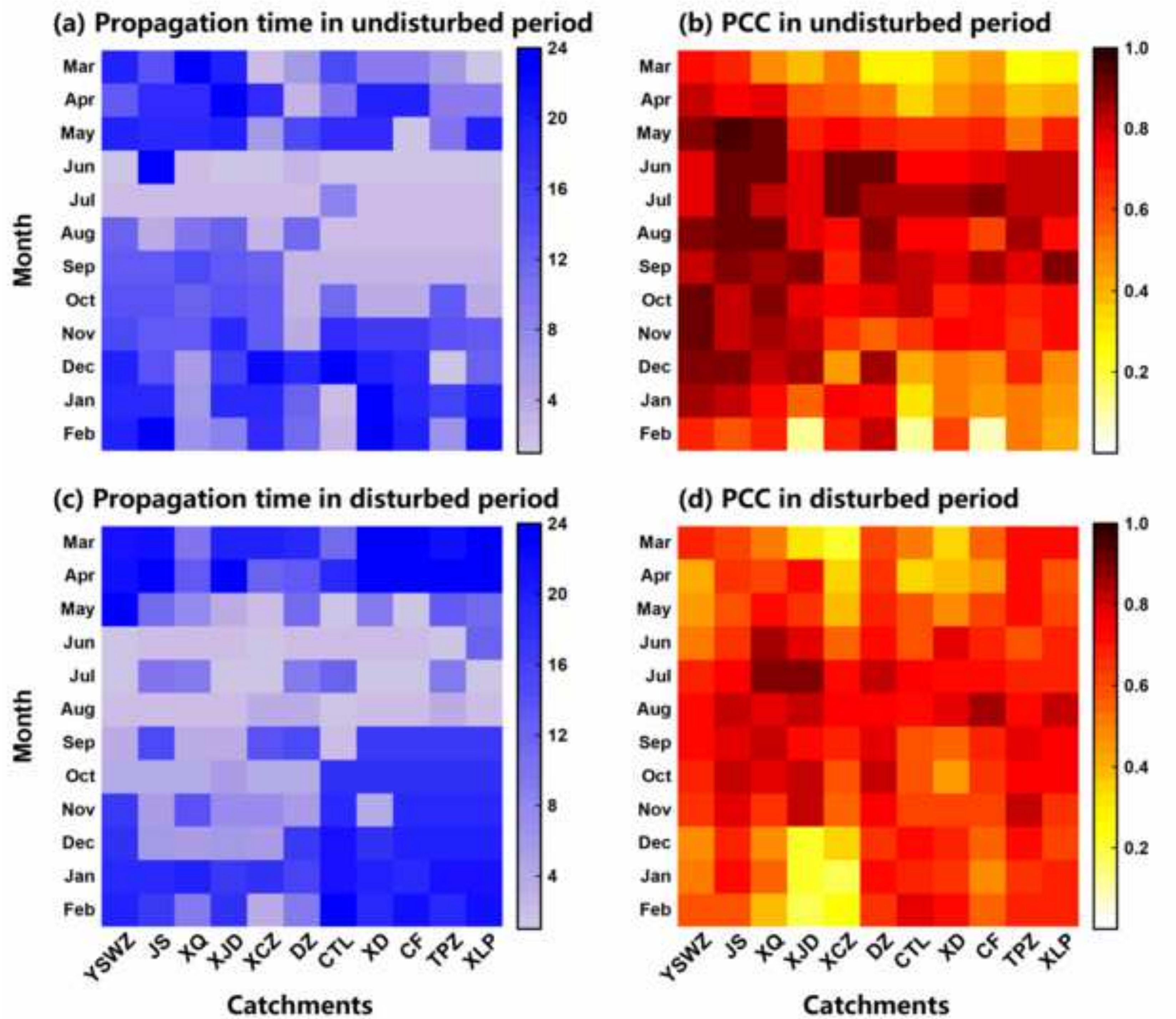

Figure10

Click here to access/download;Figure;FIG-10.tif

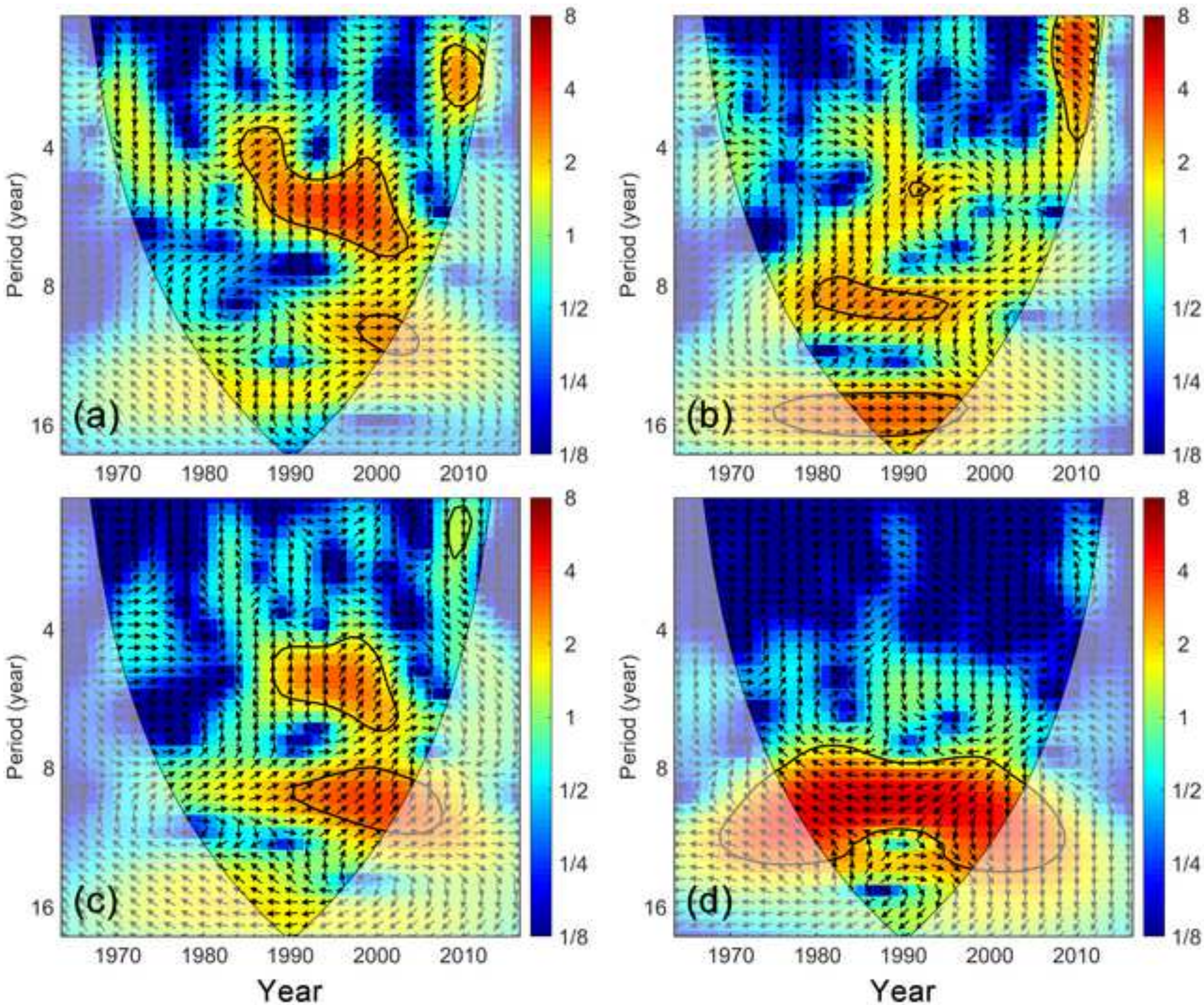

Figure11

Click here to access/download;Figure;FIG-11.tif

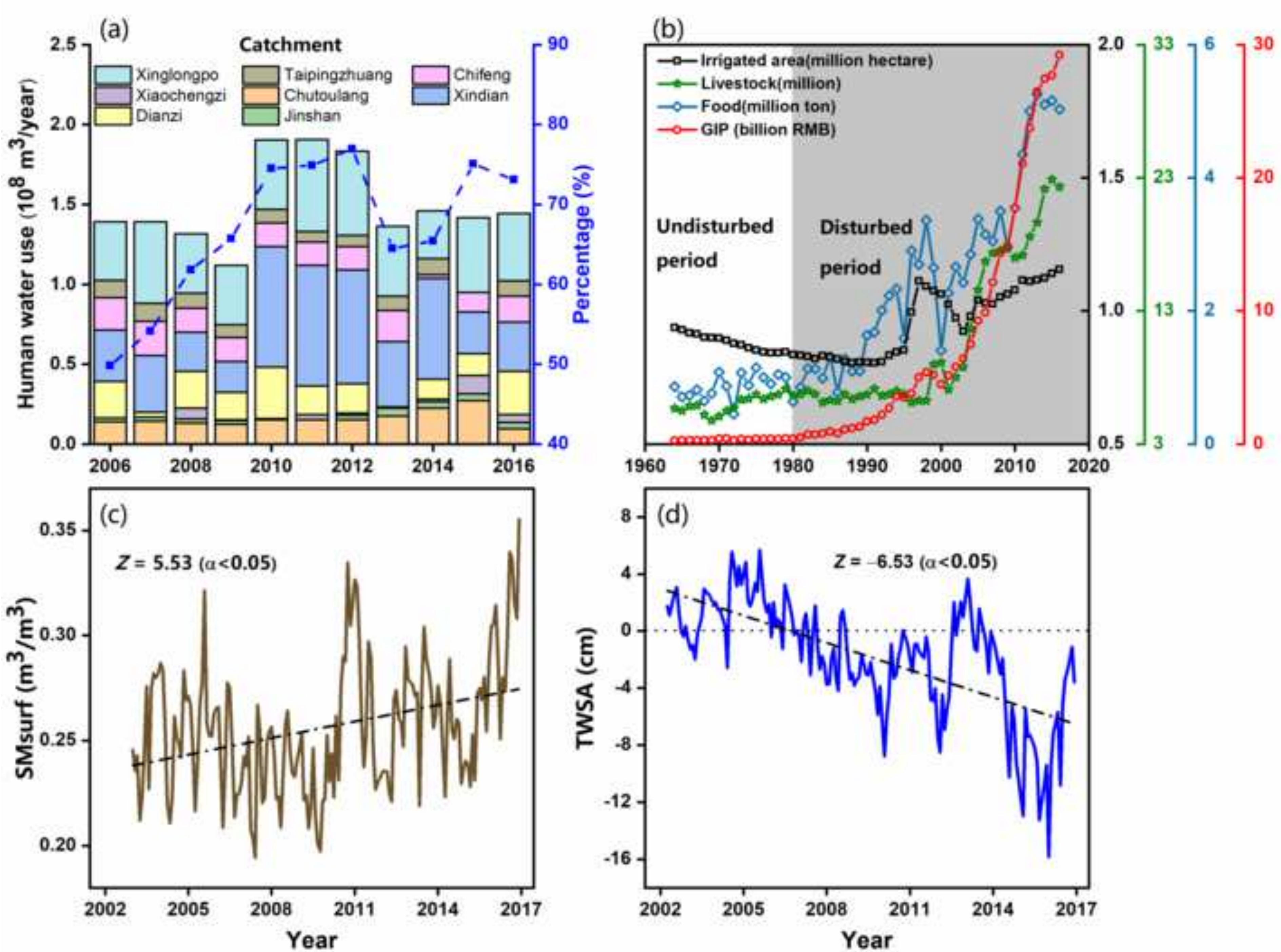

Fig. 1. Location of the Laohahe basin and distribution of hydrological, meteorological, and rain gauge stations.

Fig. 2. An observation-based natural and human-impacted catchment comparison method for separating the effects of climate change and human activities on drought propagation.

Fig. 3. Double cumulative curves of precipitation and runoff for the 11 selected catchments in the Laohahe basin.

Fig. 4. Temporal changes of socioeconomic indicators (average population (a), GDP (b), and night light (c) density), proportion of cropland and urban land (d), and human influence scores (e) for each catchment in the Laohahe basin.

Fig. 5. Spatial distribution of socioeconomic indicators, land use data and human influence scores in the Laohahe basin.

Fig. 6. Modified Mann–Kendall (MMK) trends in the long-term Standardized Precipitation Index and Standardized Runoff Index time series measured at 1-, 3-, and 12-month time scales in 11 catchments of the Laohahe basin from 1964 to 2016. The colour bar denotes the value of the *Z* statistic. “*” and “**” means significance at 0.05 and 0.01 level.

Fig. 7. Box plots of drought severity for meteorological and hydrological drought of 11 catchments in the Laohahe basin during undisturbed and disturbed periods, based on the Standardized Precipitation Index (SPI) and Standardized Runoff Index (SRI) time series measured at 3-month time scales. The numbers within the figure are the average severity of meteorological and hydrological drought.

Fig. 8. PCCs for the cross-correlation between the SRI-1 series and the SPI series at various time scales for all 11 catchments ((a) and (d) for natural catchments; (b), (c), (e), and (f), for human-influenced catchments) during undisturbed (top) and disturbed (bottom) periods. The grey shading indicates the range of time scales with the maximum PCC.

Fig. 9. Seasonal variability in the drought propagation time during (a) undisturbed and (c) disturbed periods and the corresponding maximum PCC for each month in each catchment ((b) and (d)). The colour bars indicate the drought propagation time in months (left) and the maximum PCC (right).

Fig. 10. The cross wavelet transforms between annual actual evaporation in the JS catchment and average monthly (a) ENSO, (b) AO, (c) PDO and (d) sunspot values during 1964–2016. The 95% confidence level against the red noise is exhibited as a thick contour, and the relative phase relationship is denoted as arrows (with negative

correlations pointing left and positive associations pointing right). The colour bar on the right denotes the wavelet energy.

Fig. 11. (a) Annual water withdrawal for each catchment and the percentage of total withdrawal to natural runoff for the Laohahe basin during 2006–2016, (b) changes in agricultural and industrial production data for the study area during 1964–2016 (undisturbed period and disturbed period), and time series of (c) surface soil moisture (SMsurf) and (d) terrestrial water storage anomalies (TWSA) during 2003–2016 (the *Z* value is calculated by the MMK test method).

Table 1

Characteristics of the selected catchments in the Laohahe basin.

Catchment	Hydrological station	Abbreviation	Area (km^2)	Lon (E°)	Lat (N°)	Mean annual precipitation (mm/year)	Mean annual runoff (mm/year)	Data period
1	Chutoulang	CTL	2869	118.62	42.35	402.61	26.17	1964-2016
2	Xingjude	XJD	697	118.13	42.08	422.70	39.65	1964-2016
3	Yangshuwanzi	YSWZ	674	118.17	42.07	398.97	49.46	1964-2016
4	Jinshan	JS	1034	118.68	41.92	453.60	44.03	1964-2016
5	Xiaochengzi	XCZ	866	119.00	41.75	450.57	34.89	1964-2016
6	Xiquan	XQ	419	118.53	41.42	572.88	122.80	1964-2016
7	Dianzi	DZ	1643	118.83	41.42	523.26	63.42	1964-2016
8	Xindian	XD	5580	118.70	42.33	401.50	21.50	1964-2016
9	Chifeng	CF	8678	118.95	42.28	401.00	21.06	1964-2016
10	Taipingzhuang	TPZ	7720	119.25	42.20	438.53	26.57	1964-2016
11	Xinglongpo	XLP	18112	119.43	42.32	411.74	24.48	1964-2016

Notes: The Xinglongpo streamflow station of was built in 1976, and the streamflow data before 1976 are substituted by those recorded at the adjacent Xiaoheyan station (42.32°N, 119.43°E).

Table 2

Detail information of remote sensing inversion and reanalysis data used in this study.

Data types	Temporal and spatial coverage	Units	Data sources
DEM	2012/30″	m	Refer to U.S. Geological Survey (USGS) website (https://www.usgs.gov/).
ENSO, PDO, AO	1964-2016/—	—	NOAA Physical Sciences Laboratory (PSL) (https://psl.noaa.gov/data/climateindices/);
Sunspot data	1964-2016/—	—	Royal Observatory of Belgium (http://www.sidc.be/sunspot-data)
Surface soil moisture	2003-2016/0.1°	m^3/m^3	(Chen et al., 2021) (https://doi.org/10.1594/PANGAEA.912597).
Gravity recovery and climate experiment (GRACE) data	2003-2016/0.25°	cm	GRACE RL06 CSR mascon solutions (http://www2.csr.utexas.edu/grace); (Wei et al, 2021)
Land use and cover	1980, 1990, 1995, 2000, 2005, 2010, 2015/~1 km	—	Data Centre for Resources and Environmental Sciences, Chinese Academy of Sciences (RESDC) (http://www.resdc.cn)
GDP density	2000, 2005, 2010, 2015/~1 km	million RMB/km^2	Same as Land use and cover
Population density	2000, 2005, 2010, 2015/~1 km	persons/ km^2	NASA Socioeconomic Data and Applications Center (SEDAC). (https://doi.org/10.7927/H49C6VHW)
Night light density	1995, 2000, 2005, 2010, 2013/~1 km	DN/km^2	NOAA's National Geophysical Data Center (https://www.ngdc.noaa.gov/eog/dmsp/downloadV4composites.html)

Notes: The DN value represents the average light intensity in the range of 0–63, and the larger the DN value, the higher the light intensity

Table 3

Classification and the corresponding scores of indictors reflecting human influence.

Data set	Grade	Score	Reference
Population density	0-278	1	(Perkl, 2016)
(persons/km^2)	278-390	2	
	390-501	3	
	501-612	4	
	>612	5	
GDP density	0-3	1	(Han et al., 2012)
(million RMB/km^2)	3-20	2	
	20-50	3	
	50-100	4	
	>100	5	
Night light density	0-12	0	(Small et al., 2011; Ma et al., 2012)
(DN/km^2)	>12	1	
Land cover	Cropland	3	(Theobald et al. 2010; Perkl, 2016)
	Urban land	4	
	others	0	

Note: The DN value represents the average light intensity in the range of 0–63, and the larger the DN value, the stronger the light intensity.

Table 4

Results of the trend analysis and change point tests of annual precipitation (P), PET, and runoff (R) for the selected catchments during the period of 1964–2016.

Catchments	MMK trend test (year)			Pettitt test for the change point (year)			Heuristic segmentation test for the change point (year)		
	P	PET	R	P	PET	R	P	PET	R
CTL	–1.57 ↓	–1.47 ↓	–4.46 ↓ **	—	—	1979*,1999**	—	—	1999**
XJD	–1.10 ↓	–0.97 ↓	–2.82 ↓ **	—	—	1999**	—	—	1998*
YSWZ	–0.66 ↓	–0.93 ↓	–0.40 ↓	—	—	—	—	—	—
JS	–0.65 ↓	–0.25 ↓	–0.88 ↓	—	—	—	—	—	—
XCZ	–1.00 ↓	–0.18 ↓	–4.18 ↓ **	—	—	1998**	—	—	1999**
XQ	–1.36 ↓	–1.20 ↓	–0.48 ↓	—	—	—	—	—	—
DZ	–0.51 ↓	–0.21 ↓	–1.71 ↓ *	—	—	1979**,1999*	—	—	1979*,1999*
XD	–1.33 ↓	–1.11 ↓	–3.94 ↓ **	—	—	1979**,1999**	—	—	1979**,1999**
CF	–0.72 ↓	–0.64 ↓	–4.12 ↓ **	—	—	1979*,1999**	—	—	1979*,1999**
TPZ	–0.60 ↓	0.31 ↑	–4.10 ↓ **	—	—	1979**,1999**	—	—	1979**,1999**
XJD	–0.94 ↓	–0.70 ↓	–5.04 ↓ **	—	—	1979**,1999**	—	—	1979*,1999**

Notes: ‘ ↓ ’ and ‘ ↑ ’ indicate downward and upward trends, respectively. ‘*’ and ‘**’ denote significance at the 95% and 99% confidence levels, respectively.

Table 5

Summary of average human influence scores during 2000-2015 and reservoirs information for the 11 selected catchments (human-impacted catchments are divided into two groups according to catchment area, as shown in Fig. 8).

Group	Natural catchments (catchment area < 2000 km^2)			Human-impacted catchments (I) (catchment area < 2000 km^2)			Human-impacted catchments (II) (catchment area > 2000 km^2)				
Catchment	YSWZ	JS	XQ	XCZ	DZ	XJD	CTL	XD	CF	TPZ	XLP
HI scores	2.46	2.19	1.26	3.54	3.16	3.19	3.27	3.11	7.42	6.77	7.24
Reservoir	No	No	No	No	Yes	No	Yes	Yes	Yes	Yes	Yes

Table 6

Differences in average drought characteristics calculated from SPI-3 and SRI-3 series between undisturbed and disturbed periods for the selected 11 catchments in the Laohahe basin.

Types	Catchments	Average drought duration (%)		Average drought severity (%)	
		SPI-3	SRI-3	SPI-3	SRI-3
Natural catchments	YSWZ	–3.8	41.2	–5.1	3.2
	JS	–0.6	70.7	–6.8	93.1
	XQ	6.9	30.3	13.5	35.0
	Mean	0.8	47.4	0.5	43.8
Human-impacted catchments (I)	XCZ	–3.2	224.1	–5.1	189.4
	DZ	–3.1	125.8	6.8	175.8
	XJD	12.7	–6.1	24.9	–32.2
	Mean	2.1	114.6	8.9	110.7
Human-impacted catchments (II)	CTL	11.5	26.3	25.2	52.6
	XD	1.7	123.6	18.9	232.7
	CF	8.5	263.8	18.2	418.5
	TPZ	–2.1	176.3	–10.8	653.3
	XLP	–6.6	376.2	–12.3	1236.7
	Mean	2.6	193.2	7.8	518.8

Table 7

Differences in the drought propagation time for different comparison schemes.

Comparison schemes	Period	Catchments types	Drought propagation time (months)		
			Mean	Median	Max.
I	Undisturbed	Natural	12.7	12.0	14.0
	——	Human-impacted (I)	9.0	9.0	12.0
	Difference	(months)	–3.0	–3.0	–2.0
	——	Human-impacted (II)	10.4	11.0	12.0
	Difference	(months)	–2.0	–1.0	–2.0
Ⅱ	Undisturbed	Natural	12.7	12.0	14.0
	Disturbed	Natural	9.3	9.0	11.0
	Difference	(months)	–3.0	–3.0	–3.0
Ⅲ	Disturbed	Natural	9.3	9.0	11.0
	——	Human-impacted (I)	11.3	11.0	12.0
	Difference	(months)	+2.0	+2.0	+1.0
	——	Human-impacted (II)	21.0	20.0	23.0
	Difference	(months)	+12.0	+11.0	+12.0

Note: Propagation time indicates the SPI accumulation period (SPI-n) most strongly correlated with SRI-1. A negative change (–) means that the SPI accumulation period becomes shorter; a positive change (+) means that the SPI accumulation period becomes longer.